1 Title

DynaMiTES - a dynamic cell culture platform for in vitro drug testing PART 2 – *Ocular* DynaMiTES for drug absorption studies of the anterior eye

2 Authors

Nicole Beißner [1,3*], Kai Mattern [2,3*], Andreas Dietzel [2,3], Stephan Reichl [1,3]

[1] Institut für Pharmazeutische Technologie, Technische Universität Braunschweig, Mendelssohnstraße 1, 38106 Braunschweig, Germany

[2] Institut für Mikrotechnik, Technische Universität Braunschweig, Alte Salzdahlumer Straße 203, 38124 Braunschweig, Germany

[3] Center of Pharmaceutical Engineering – PVZ, Technische Universität Braunschweig, Franz-Liszt-Straße 35 A, 38106 Braunschweig

* These authors contributed equally to this work

3 Address for Correspondence

PD Dr. Stephan Reichl, Institut für Pharmazeutische Technologie, Technische Universität Braunschweig, Mendelssohnstraße 1, 38106 Braunschweig, Germany

E-Mail: s.reichl@tu-braunschweig.de

Fon: 0531-391 5651

Fax: 0531-391 8108

https://doi.org/10.24355/dbbs.084-201904011253-0

4 Abstract

In the present study, a formerly designed Dynamic Micro Tissue Engineering System (DynaMiTES) was applied with our prevalidated human hemicornea (HC) construct to obtain a test platform for improved absorption studies of the anterior eye (*Ocular* DynaMiTES). First, the cultivation procedure of the classic HC was slightly adapted to the novel DynaMiTES design. The obtained inverted HC was then compared to classic HC regarding cell morphology using light and scanning electron microscopy, cell viability using MTT dye reaction and epithelial barrier properties observing transepithelial electrical resistance and apparent permeation coefficient of sodium fluorescein. These tested cell criteria were similar. In addition, the effects of four different flow rates on the same cell characteristics were investigated using the DynaMiTES. Because no harmful potential of flow was found, dynamic absorption studies of sodium fluorescein with and without 0.005 %, 0.01 % and 0.02 % benzalkonium chloride were performed compared to the common static test procedure. In this proof-of-concept study, the dynamic test conditions showed different results than the static test conditions with a better prediction of in vivo data. Thus, we propose that our DynaMiTES platform provides great opportunities for the improvement of common in vitro drug testing procedures.

5 Keywords

DynaMiTES, human hemicornea construct, microfluidic system, organ on chip, TEER measurement, dynamic flow system, in vitro drug absorption, benzalkonium chloride

https://doi.org/10.24355/dbbs.084-201904011253-0

6 Introduction

The development of novel drugs or innovative formulations is both cost intensive and time consuming. Thus, much effort is spent in the early phases of this process to obtain reliable findings. Unfortunately, most common preclinical test systems are based on animal experiments, ex vivo or in vitro models utilizing cell cultures, which all have well-known disadvantages. For example, the application of animals is ethically questionable and rarely representative for the effect in humans [5,21,40]. Furthermore, ex vivo as well as in vitro experiments are usually performed under static conditions, which cannot adequately mimic the physiological conditions in humans. Consequently, misleading outcomes often result in late stage drug failure. For this reason, scientists have been working for decades on improved in vitro methods for the early and reliable selection of the most important and promising drug candidates. One tremendous innovation in this field was the development of organ on chip (OOC) systems in the early 2010s [3,22,55]. In these microstructured systems, well-characterized cell cultures can be cultured within small dimensions under a highly controlled microenvironment. These features should ease the in vitro emulation of human physiology and may ultimately lead to more reliable results [5,10,32,49].

Despite great hope, OOC systems also exhibit essential disadvantages. On the one hand, they are poorly compatible with well-known cell culture systems. Thus, cell culture laboratories, which have long-term experience with in vitro models, cannot easily adapt them to OOC systems. Consequently, new efforts must be made to this purpose. Other dynamic systems, which enable the integration of standard cell culture models, such as the Quasi Vivo® system (Kirkstall, Rotherham, UK), do not provide additional analysis, such as continuous **t**rans**e**pithelial **e**lectrical

https://doi.org/10.24355/dbbs.084-201904011253-0

65 **r**esistance (**TEER**) measurement [26], as OOCs try to include [6]. On the other hand,
66 the most commonly used material for OOC fabrication, polydimethylsiloxane (PDMS),
67 is known for its intensive substance absorption [39,45]. In research, it is used due to
68 its easy structurability even with challenging geometries, its transparency, its
69 biocompatibility and its gas permeability. However, substance absorption can hinder
70 cell nutrition and, more importantly, the detection of drugs. For these reasons, PDMS
71 is not an ideal material for routinely used absorption test systems of strong
72 physiological and poorly permeated barriers, such as the human cornea.

73 Against this background, our interdisciplinary team of engineers and pharmacists has
74 developed a microstructured system for dynamic in vitro drug absorption tests that
75 circumvents these disadvantages and allows the integration of standard cell culture
76 inserts and includes continuous TEER measurement. The resulting **Dyna**mic **Mi**cro
77 **T**issue **E**ngineering **S**ystem (**DynaMiTES;** see Figure 1) was built for dynamic cell
78 cultivation and, more importantly, the dynamic drug absorption testing on
79 physiological barriers.

80 One pharmaceutically challenging physiological barrier is the human cornea. Ocular
81 drug absorption is hindered to a great extent due to very tight cell-cell connections
82 and short precorneal residence time because of tear flow [4,23]. Unfortunately,
83 common ocular test systems apply static test conditions and thus fail to reliably
84 emulate the dynamic human physiology. Consequently, the harmful effects of
85 excipients, such as preservatives, might have a stronger effect on the permeated
86 drug amount than in the clinical application. As no dynamic setup for cell culture
87 models has been reported to date, an *Ocular* DynaMiTES for the implementation of
88 in vivo-like conditions in pharmaceutical formulation testing would be the first step
89 toward significantly improving the common test practice. Unlike static test systems,

https://doi.org/10.24355/dbbs.084-201904011253-0

the enhanced dynamic system might not overestimate increased drug absorption resulting from non-physiological harmful conditions or toxic effects. For this reason, a dynamic test procedure will ensure an improved emulation of the in vivo situation and may offer a significant contribution to more reliable preclinical in vitro test systems [37].

For the generation of an *Ocular* DynaMiTES, our well-characterized and prevalidated human hemicornea (HC) construct [19,20] was applied within the DynaMiTES. In our first study, the technical design was tested and simulated intensively. Furthermore, the cell compatibility of all applied materials was investigated (see PART 1). Based on these findings, our second study (PART 2) focused on the cellular component - the HC construct. First, the cultivation of the HC had to be slightly adapted due to the DynaMiTES design. The resulting inverted HC was then compared to the classic HC with regard to cell morphology, cell viability, TEER value and apparent permeation coefficient (P_{app}) of sodium fluorescein as a paracellular marker substance to ensure similar cell characteristics. Second, absorption studies with sodium fluorescein were performed within the DynaMiTES with and without flow conditions. In this manner, potential harming or biasing effects of the materials and the engineering design could be examined. For this reason, four different flow rates were tested concerning cell viability, cell morphology, TEER value and P_{app}. After successfully performing this stepwise alteration of the common static in vitro practice, the first donor dilution experiments with and without a common ocular permeation enhancing preservative, benzalkonium chloride (0.005 %, 0.01 % and 0.02 %) [9,24,41], were performed to demonstrate the benefits of our dynamic test system. Taken together, these studies should show the importance and readiness of the *Ocular* DynaMiTES for application in improved drug absorption studies of the anterior eye.

https://doi.org/10.24355/dbbs.084-201904011253-0

7 Materials and Methods

7.1 Materials

Cell culture flasks and Transwell® inserts (art. no. 3402) were purchased from Sarstedt (Nümbrecht, Germany) and Corning Costar (Kennebunk, Maine, US), respectively. The Keratinocyte Growth Medium (KGM), which emerged from the Keratinocyte Basal Medium (KBM) by the addition of SingleQuots®, was provided from Lonza (Basel, Switzerland). KCl and $MgSO_4 \times 7\ H_2O$ were acquired from Acros Organics (Geel, Belgium). Phosphate Buffered Saline (PBS) tablets and EDTA disodium salt solution were obtained from MP Biomedicals (Santa Ana, California, US). Trypsin-EDTA and trypsin inhibitor were acquired from Thermo Fisher Scientific (Waltham, Massachusetts, US). The acetic acid, NaCl, $NaHCO_3$, HEPES, ascorbic acid, D-glucose monohydrate, $CaCl_2 \times 2\ H_2O$, sodium dodecyl sulfate (SDS), formaldehyde 4 % solution, glutaraldehyd 25 % solution, osmiumtetroxid 2 % solution and hematoxylin solution were purchased from Carl Roth (Karlsruhe, Germany). Technovit 7100 was obtained from Heraeus Kulzer (Wehrheim, Germany). The $NaH_2PO_4 \times H_2O$ and the L-glutamine were provided by Merck (Darmstadt, Germany). Sodium fluorescein, hydrochloric acid, 10-fold MEM and 3-(4,5-Dimethyl-2-thiazolyl)-2,5-diphenyl-2H-tetrazolium bromide (MTT) were purchased from Sigma-Aldrich (Munich, Germany). Benzalkonium chloride (BAC) 50 % solution was purchased from Caelo (Hilden, Germany). The PCR mycoplasma test kit for routinely mycoplasma screening was bought from Promocell (Heidelberg, Germany). The collagen for the three-dimensional gel was extracted from rat tail following a standard protocol. The employed Krebs-Ringer buffer (KRB) contained 6.8 g NaCl, 0.4 g KCl, 0.14 g

https://doi.org/10.24355/dbbs.084-201904011253-0

$NaH_2PO_4 \times H_2O$, 2.1 g $NaHCO_3$, 3.575 g HEPES, 1.1 g D-glucose monohydrate, 0.2 g $MgSO_4$ x 7 H_2O and 0.26 g $CaCl_2 \times 2\ H_2O$ in 1000 mL of double-distilled water.

7.2 Cultivation of Human Corneal Epithelial (HCE-T) Cells

The HCE-T cell line originated from a 49-year-old female and was immortalized by transfection with a recombinant SV40-adenovirus vector. This establishment and the subsequent characterization were performed by Araki-Sasaki et al. [2]. The HCE-T cells for the following study were purchased from the RIKEN cell bank (Tsukuba, Japan) and cultured with KGM at 37 °C and 5 % CO_2 in a humidified atmosphere.

7.3 Cultivation of Human Corneal Keratocytes (HCK) Cells

The HCK cell line was also immortalized by transfection with an SV40-adenovirus vector but derived from human corneal keratocytes [20,57]. For the cultivation of our HC, HCK cells were provided by Dr. M. Zorn-Kruppa (Hamburg, Germany) and cultured with KGM under the same conditions as HCE-T cells.

Both cell types were routinely tested for mycoplasma infection.

7.4 Cultivation of Human Hemicornea (HC) Construct

For the combination of our well-known HC construct and novel DynaMiTES as an *Ocular* DynaMiTES, the cultivation of HC was slightly adapted. Due to the insert orientation within the DynaMiTES (see Figure 2) and to ensure fluid flow over the corneal epithelium, HCE-T cells were grown on the bottom side of the insert membrane. For this reason, the HC for the DynaMiTES was cultured inversely in contrast to the classic culture conditions of Hahne et al. [19,20] (see Figure 3).

For the classic HC, HCK cells within a collagen stroma matrix and HCE-T cell lines placed on top of the HCK cells were cultured with KGM under serum-free conditions on permeable polycarbonate Transwell® filters at 37 °C and 5 % CO_2 in a humidified

https://doi.org/10.24355/dbbs.084-201904011253-0

atmosphere as described by Hahne et al. [19,20]. For the inverted HC, the collagen gel production was identical to the classic HC but different from the classic cultivation the Transwell® inserts were placed upside down into a 6-well plate after the gelling process. A HCE-T cell suspension of 100,000 cells/200 µL was then applied to the bottom surface of every insert. After cell adhesion for 1 h, 3 h or overnight (18 h), the inserts were reversed and cultured until day 7 similar to the classic HC protocol. On day 7, all HCs were lifted to an air-liquid interface to induce an epithelial multilayer. The inverted HCs were once more inverted to the 6-well plate and fed daily with KGM from underneath the insert. For optimal cell nutrition, the inserts were always carefully tilted to avoid air accumulation under the collagen gel.

7.5 Technical Design of the DynaMiTES

As the technical component of our ocular system, the DynaMiTES consist of three separate levels: bottom level, insert level and top level (see Figure 1; for technical development and fabrication see PART 1). All these levels are built from polycarbonate (PC). Because the DynaMiTES was designed for repeated use, unlike common OOCs, the PC fabrication ensures enhanced durability and low substance absorption [51]. Furthermore, the modular design with its three levels enables individualization for a wide range of cell culture laboratories and their in vitro models. For example, the insert level can be adapted to different insert geometries, whereas the top and bottom levels, which are more elaborate to produce, can remain unchanged. The customizable insert level also consists of a sampling point to access the acceptor, which is situated between the insert and bottom levels. Acceptor and donor volumes were designed similar to common in vitro tests, at 1600 µL and 370 µL, respectively. Furthermore, the microstructured donor channel with its posts ensures optimal mixing conditions (for channel construction and flow simulation see

https://doi.org/10.24355/dbbs.084-201904011253-0

PART 1). However, this design is the opposite of the common test procedure, where the donor is applied in the insert and the acceptor is provided beneath the insert (see Figure 2 and Figure 6). This change was important to ensure in vivo-like fluid flow across the cellular surface. Additionally, it eases dynamic donor variation, such as donor dilution, mimicking physiological concentration gradients. Moreover, it allows further downsizing of the channel dimensions for subsequent improvements to even closer emulate human physiology. In addition to donor variation, TEER electrodes built from stainless steel were included in the top and bottom levels. These additions allow continuous TEER measurement and provide real-time information of the substance-barrier interaction.

After successfully testing the cell compatibility (see PART 1) and cell characteristics of the inverted HC (see Section 8.1), flow conditions were simulated using the DynaMiTES. A basal flow rate (31 µL/min) and an initial flow rate (73 µL/min), whereby the latter emulates the increased tear flow after instillation, were chosen following Sörensen and Taagehöj [43] and calculated for the donor volume of 370 µL (see PART 1). In addition, a slightly elevated flow rate (93 µL/min) and doubled initial flow rate (148 µL/min) were applied to investigate method limits. The effect of these flow rates on cell morphology, cell viability, TEER and P_{app} was investigated using the following methods. As a negative control, inverted HC in the standard well plate (0 µL/min well plate) and in the DynaMiTES without flow (0 µL/min DynaMiTES) were investigated in parallel.

https://doi.org/10.24355/dbbs.084-201904011253-0

7.6 Cell Morphology

7.6.1 Light Microscopy (LM)

For light microscopic observation of tissue cross sections using an Olympus IX50 photomicroscope (Olympus, Hamburg, Germany), the HCs were fixed with a phosphate buffered solution of 4 % formaldehyde for 24 h and subsequently dehydrated with an ethanol series. Next, the HCs were cut into two halves, and each half was embedded in a plastic resin on a base of hydroxyethylmethylacrylate (Technovit 7100) according to the manufacturer's protocol. This resin block was cut in 3.5-µm-thick slices, which were stained using hematoxylin and eosin.

7.6.2 Scanning Electron Microscopy (SEM)

For electron microscopic observation of the epithelial surface area using LEO 1550 (Zeiss, Oberkochen, Germany), the HCs were fixed with a 4 % solution of glutaraldehyde for 90 min and post-fixed with a 2 % solution of osmium tetroxide for 2 h. Subsequently, the tissue was dehydrated employing an ethanol series and air-dried overnight. After this drying process, the Transwell® membrane was immobilized on an SEM sample holder, and the epithelial surface was coated with gold using Bal-Tec SCD 050 (Balzer, Wiesbaden, Germany).

For the morphological evaluation of flow effects, inverted HCs in the standard well plate (0 µL/min well plate) and in the DynaMiTES without flow (0 µL/min DynaMiTES) served as a negative control. In contrast, inverted HCs whose epithelium was scratched with a glass pipette were treated equally as a positive reference.

7.7 Cell Viability

Cell viability was investigated by using an MTT dye reaction. For this purpose, the apical and basolateral side of the HC were exposed to a 1+4 mixture of MTT stock

https://doi.org/10.24355/dbbs.084-201904011253-0

solution (5 mg/mL) and KGM. After three hours of reaction at 37 °C, 5 % CO_2 and humidified atmosphere, the MTT solution was removed. For cell lysis, a lysis solution containing 2.73 g SDS, 3.64 g hydrochloric acid, 88.18 g water and 905.45 g isopropanol was applied to both sides of the HC and incubated overnight. Next, an aliquot was diluted 1+3 with fresh lysis solution, and absorption was measured at 570 nm using an UV-VIS plate reader Powerwave XS from BioTek (Winooski, Vermont, US). On the basis of these results, cell viability was calculated in relationship to an untreated reference in a well plate.

To investigate the effect of flow, the inverted HCs were set into the DynaMiTES insert level. Next, different flow rates of KRB were applied for the intended experimental duration of three hours. Cell viability was then assessed as previously described.

7.8 Transepithelial Electrical Resistance

TEER measurement during cultivation, as well as prior to and during the absorption studies, was performed using EVOM® combined with Endohm® Chamber from World Precision Instruments (WPI, Sarasota, Florida, US). For TEER measurement within the DynaMiTES, the incorporated electrodes were connected to the EVOM®, and TEER was measured on every sampling point of the absorption study. For the TEER profiles, the starting TEER value of every HC was set as 100 %, and the subsequent values were calculated in relationship to the starting value.

As a negative control, the TEER profiles of inverted HCs in a normal well plate were assessed simultaneously for each experiment. Biasing effects on the TEER measurement resulting from the DynaMiTES construction or the flow itself were investigated with a positive control. For this reason, inverted HCs were devitalized with a solution of 0.03 % SDS over 3 h prior to the experiment. Subsequently, the

https://doi.org/10.24355/dbbs.084-201904011253-0

TEER profiles were analyzed over 180 min with a flow rate of 31 µL/min. Because no base line shift was observed, biasing effects of the DynaMiTES cannot be expected (data not shown).

7.9 Static Absorption Studies

In addition to TEER, the absorption of sodium fluorescein as a hydrophilic and paracellular marker substance [31] was used for the evaluation of epithelial barrier properties. All absorption studies were performed in KRB according to the prevalidation study of the classic HC [20]. The donor solution (250 µg/mL sodium fluorescein in KRB) was applied to the epithelial surface at day 10 of cultivation (see Figure 6A), and the amount of permeated sodium fluorescein in the acceptor compartment was detected over the course of 180 min. All acceptor samples were analyzed using a fluorescence microplate reader Genios from Tecan (Männedorf, Switzerland) at an excitation wavelength of 485 nm and an emission wavelength of 535 nm. From the obtained concentrations, the amount of permeated sodium fluorescein was calculated and plotted over time. The linear ascent of these permeation profiles was then used to calculate the apparent permeation coefficient (P_{app}) as described by Hahne et al. [20].

For absorption studies within the DynaMiTES, the inlet of every system was connected with a syringe pump (KDS 270 Legacy Syringe Pump, KD Scientific, Holliston, Massachusetts, US). The donor compartment was then either filled once with the donor solution (250 µg/mL sodium fluorescein) for the simulation of classic static test conditions or the donor was pumped along the epithelial surface with four different flow rates for flow effect investigation (see Figure 2 and Section 7.5).

https://doi.org/10.24355/dbbs.084-201904011253-0

7.10 Static vs. Dynamic Absorption Studies

The dynamic absorption studies were performed with a 10-fold higher concentration of sodium fluorescein (2.5 mg/mL) to ensure acceptor concentration above the detection limit. After a single donor filling (bolus application), an initial flow rate of KRB (73 µL/min) was applied for 5 min to simulate elevated tear drainage after instillation [33,43]. Subsequently, a basal flow of KRB (31 µL/min) was applied for 175 min. Acceptor samples were obtained and analyzed similar to the static absorption studies. In parallel, static experiments without KRB dilution were performed in the DynaMiTES with the same donor solution.

As a proof-of-concept, the comparison of static and dynamic test conditions was further performed after exposure to 0.005 %, 0.01 % and 0.02 % BAC in KRB. To avoid BAC and sodium fluorescein interaction, both substances were applied consecutively. In the first phase, the HC was exposed to a specific BAC solution. For dynamic exposure, BAC was diluted by KRB flow (5 min 73 µL/min and 25 min 31 µL/min) after a bolus application. A second flow regime with 10 min of 73 µL/min and 20 min of 31 µL/min was tested with the highest BAC concentration to investigate the flow rate effect (0.02 % EF = elevated flow). In static experiments, the donor remained unchanged for 30 min. In the second phase, the sodium fluorescein permeation was performed similar to the dynamic absorption studies over the course of 180 min. Dynamic BAC exposure was always followed by dynamic sodium fluorescein permeation to simulate the novel dynamic test conditions. In contrast, static BAC exposition was followed by static sodium fluorescein permeation to recreate common static test procedures. For the latter, the P_{app} was calculated from the linear ascent as previously described (see Section 7.9). In the dynamic experiments, this was not feasible due to the lack of infinite dose. Thus, the acceptor

https://doi.org/10.24355/dbbs.084-201904011253-0

concentrations of sodium fluorescein were utilized for a comparison of the dynamic conditions.

7.11 Statistical Analysis

Statistical analysis was performed using IBM SPSS Statistics 24 (IBM, Armonk, New York, US). Differences between two groups were compared using independent two-sample t-test. More than two groups were investigated using one-way ANOVA (**an**alysis **o**f **va**riance). For detailed distinction, of differences found in ANOVA the Bonferroni *post hoc* test was used for homogeneous variance and the Games-Howell *post hoc* test for inhomogeneous variances. p-values of less than 0.05 were considered significant ($p < 0.05$*, $p < 0.01$**).

8 Results

8.1 Adaption of HC Cultivation to the DynaMiTES Design

As previously discussed, the HC cultivation was adapted for the application of the HC construct within the DynaMiTES. The resulting inverted HC were then compared to the classic HC with regard to cell morphology, cell viability, TEER and P_{app} to ensure similar cell characteristics.

8.1.1 Cell Morphology

A variation in attachment time (1 h, 3 h und 18 h) for the epithelial cells of the inverted HC displayed an increasing number of epithelial layers with increasing attachment time (see Table 1). However, morphology similar to the classic HC was best obtained with overnight attachment. Classic as well as inverted HC showed both tight epithelial cell growth with two to more cell layers under these conditions (see Figure 3). Thus, overnight attachment was used for all following experiments.

https://doi.org/10.24355/dbbs.084-201904011253-0

8.1.2 Cell Viability

Cell viability of classic and inverted HC were compared using MTT dye reaction. As a positive reference, a group of stroma equivalents without HCE-T cells and only containing HCK cells was cultured simultaneously. On day 10 of cultivation, classic as well as inverted HC showed cell viabilities of or close to 100 %, which were not significantly different from each other. In contrast, the cell viability of the positive reference was significantly diminished, caused by HCE-T cell exclusion (see Figure 4).

8.1.3 Transepithelial Electrical Resistance

In addition to cell morphology and cell viability, TEER values were measured on cultivation day 6, the day before ALI (see Figure 3), and until day 13. In this manner, changes in the epithelial barrier resulting from the ALI cultivation could be investigated over an extended period of eight days (see Figure 5). Within this time span, the classic HC showed higher TEER values at the beginning, which decreased constantly during ALI cultivation. In contrast, the inverted HC showed decreasing TEER values, which increased after the beginning of ALI cultivation. Despite these differing TEER developments in the early phases of cultivation, classic as well as inverted HC showed similar TEER values on day 10, the day of application for absorption studies following Hahne et al. [20]. An extended cultivation did not show any significantly different TEER values for the following three days. A TEER optimum was reached between day 10 and day 11 for the inverted HC, which was similar to the findings observed by Hahne and Reichl for classic HC in 2011 [19].

8.1.4 Absorption Studies

Following the absorption studies of Hahne et al. [19,20], the P_{app} of sodium fluorescein was analyzed on day 10 of cultivation for the inverted as well as for the

https://doi.org/10.24355/dbbs.084-201904011253-0

353 classic HC. As the similar TEER values might have indicated, the obtained P_{app}
354 values were also not significantly different between both groups. Moreover, the
355 values were similar to the values for the classic HC published by
356 Hahne et al. [20] (see Figure 6).

357 8.2 Absorption Studies with and without Flow in the DynaMiTES

358 After successfully adapting the HC's cultivation for the novel design, the potential
359 harmful effects of fluid flow should be investigated prior to the application of dynamic
360 experimental test conditions. For this reason, cell morphology, cell viability, TEER
361 and P_{app} of the inverted HC were analyzed with and without utilizing different flow
362 rates.

363 8.2.1 Cell Morphology

364 Cell morphology was observed using LM for the investigation of cell abrasion or
365 alterations in cell layer formation. Furthermore, SEM was used for an extensive
366 observation of the epithelial surface to detect randomly occurring changes in the
367 epithelium.

368 In LM, neither cell detachment nor hole formation as a consequence of the applied
369 fluid flows were observed (see Table 2; left column). All images showed a
370 multilayered epithelium with a more or less uneven surface, which may have resulted
371 from the loss of contact inhibition as previously demonstrated for other SV-40
372 immortalized cell lines [30,44] or the fact that in contrast to the in vivo situation all cell
373 layers are proliferating. Furthermore, the lack of lid movement and desquamation
374 may have caused a less smooth and compact surface. However, all appearances in
375 the DynaMiTES regardless of flow were similar to the negative control in the well

https://doi.org/10.24355/dbbs.084-201904011253-0

plate. Moreover, a clear scratch in the deliberately injured positive control was visible and demonstrated that changes in cell morphology would be detectable.

In the SEM images, a similar observation could be obtained (see Table 2, right column). The samples with and without flow from the DynaMiTES showed no hole formation, as no PC membrane was visible in any of the samples areas. However, an intended injury, and thus the underlying PC membrane were clearly visible in the positive control. By locating the injury close to the margins, we were able to demonstrate that it is possible to detect mechanical injuries close to the insert edges using SEM imaging. Regarding the cellular surface, uneven cell areas were observed similar to the LM images. Overall, only a slight tendency toward a more defined surface structure could be observed with an increasing flow rate. The irregular surface in the image of the flow rate (93 µL/min), which was not observed in other samples, may be caused from the sample preparation.

8.2.2 Cell Viability

In addition to cell morphology, cell viability was examined after three hours of flow exposition. Because this was the expected experimental time for subsequent drug absorption studies, cell viability should not be restricted by shear stress or other effects during this period. A negative control was maintained in KRB in a standard well plate. Furthermore, a group of inverted HCs were inserted into the DynaMiTES, and no flow was applied (0 µL/min). The results in Figure 7 underline that no clear reduction in cell viability was found as all groups showed values above 90 % regardless of the tested flow rate.

8.2.3 Transepithelial Electrical Resistance

The integrated TEER electrodes of the DynaMiTES were used to investigate TEER development over the experimental time of 180 min. Thus, the relative TEER value

https://doi.org/10.24355/dbbs.084-201904011253-0

was obtained with and without flow over the course of 180 min (see Figure 8). As a negative control, the TEER development of inverted HCs in a cell culture well plate was analyzed simultaneously for every batch.

When comparing the inverted HCs, a slight but constant decreasing trend could be observed in the negative control. Resulting from this decrease, all groups from the DynaMiTES (except 73 µL/min) were significantly different to 0 µL/min well plate ($p < 0.05$) after 180 min but not to 0 µL/min DynaMiTES. Furthermore, a flow rate of 73 µL/min showed a short decrease in TEER value within the first 10 min and a stable value afterwards. All other flow rates initially showed ascending and subsequently stable TEER profiles. From these flow rates, the inverted HCs, which were exposed to 93 µL/min, showed the highest relative TEER value.

8.2.4 Absorption Studies

As a second parameter for the evaluation of epithelial barrier properties, the P_{app} of sodium fluorescein was accessed in the DynaMiTES with and without the application of different flow rates. As a negative control, an absorption study in a well plate was performed simultaneously in every experiment. The obtained P_{app} values are shown in Figure 9. The inverted HCs from the DynaMiTES showed all and, regardless of the flow no significant increase in P_{app} compared to the reference in the well plate. Only an injury, resulting from a static exposition to 0.01 % BAC, had significantly increased the determined P_{app}.

8.3 Dynamic Absorption Studies in the DynaMiTES

After the investigation of all harmful or interfering effects, the DynaMiTES was utilized for a small proof-of-concept study. Because, the system should emulate physiological tear drainage and thus enable the reliable evaluation of ocular drug absorption at the

https://doi.org/10.24355/dbbs.084-201904011253-0

anterior eye, the effect of divers benzalkonium chloride concentrations were investigated under static and dynamic experimental conditions.

8.3.1 Static vs. Dynamic Absorption Studies

The obtained results (see Figure 10) for sodium fluorescein without BAC addition showed a typical linear concentration-time curve for the static test conditions after reaching a steady state. In contrast, dynamic test conditions showed a lower curve, which flattened until the end of the experiment.

Following exposure to 0.005 % BAC, the curves for both conditions were similar to the curves without BAC. For the concentration of 0.01 % BAC, an increase in permeability (P_{app}) could only be detected for the static procedure ($2.83 \times 10^{-7} \pm 0.09 \times 10^{-7}$ cm/s without BAC vs. $12.2 \times 10^{-7} \pm 6.91 \times 10^{-7}$ cm/s for 0.01 % BAC - 4.3-fold increase in P_{app}), whereas no increase was found under dynamic conditions. When applying 0.02 % BAC, the curves for static ($12.6 \times 10^{-7} \pm 2.09 \times 10^{-7}$ cm/s - 4.5-fold increase in P_{app}) and dynamic conditions (10.3-fold increase in concentration) were both increased compared to the curves without BAC. Furthermore, the static curves for 0.01 % and 0.02 % BAC were comparable and showed no further increase in sodium fluorescein concentration with increasing BAC concentration. In contrast to the other curves, the two conditions both showed dramatically shortened lag phases in the beginning and had flattened over the entire experimental time.

However, the increase in dynamic concentration profile could not be observed for 0.02 % BAC with the second flow regime involving an extended initial flow rate phase (1.6-fold increase in concentration with 0.02 % BAC EF = elevated flow).

https://doi.org/10.24355/dbbs.084-201904011253-0

9 Discussion

9.1 Adaption of HC Cultivation

The four cell characteristics, morphology, viability, TEER and P_{app}, which were observed in this study together indicated that an alteration in the cultivation procedure did not significantly affect the tested criteria of our HC. The HCE-T cells on the bottom surface of the membrane developed an epithelium with 2-4 cell layers, suggesting similar epithelial barrier properties (TEER and P_{app}). Other inverted cultivations without prior coating have been previously described for Calu-3 cells and MDCK II cells in a lung model [7] and kidney model [56], respectively. However, to the best of our knowledge, cultivation on the bottom surface of the insert has not yet been reported for corneal cells, specifically HCE-T. A slightly different inverted cultivation has been published by Zorn-Kruppa et al. [57]. However, their cultivation of HCE-T cells within the insert does not allow direct flow exposition to the epithelium. For this reason our inverted cultivation is more suitable for the intended in vivo-like conditions within the DynaMiTES.

Furthermore, in the study of Bur et al., the cells were left to adhere for 48 h [7], which is longer than in our protocol, although a larger medium volume of 500 µL (compared to 200 µL) was used. To apply this larger volume, tubes were placed over the insert. Advantageously, these tubes, which may harm the cell layer when removed, were avoided in our protocol. Moreover, our overnight adhesion was longer than the 5-h time period examined in the study of Wakabayashi et al. [56]. Nevertheless, no harming effects were detected in the MTT test, as the initial seeding volume of 200 µL was higher than the 100 µL in the study of Wakabayashi et al. and our

https://doi.org/10.24355/dbbs.084-201904011253-0

collagen gel was generated using 10-fold MEM and thus ensured cell nutrition until the next day.

Morphologic observations demonstrated that the two cell types could grow in physical proximity. The cells might interact even through the PC membrane as the pore size of 3 µm is much wider than the molecule size of cytokines and other signal molecules. For this reason, the benefit of co-cultivation remains unchanged and, thus, other cell characteristics, such as substance transport [52–54] and substance metabolism [27,28], which we investigated extensively in our former studies, might also be maintained. This finding was also supported by the cell viability results. Classic and inverted HC showed both similar values. Only the value of the stromal equivalents was higher than it might be estimated by the initial cell seeding density [19]. However, this may result from a higher metabolic activity of the HCK cells compared to the HCE-T cells.

With regard to the TEER observation, the differences in the early TEER development between classic and inverted HC are of minor interest, as all models were not used until day 10 of cultivation and upon completed formation of the epithelial multilayer. Furthermore, the late TEER values, including the TEER optimum from day 10 to day 11 as well as the P_{app} values were comparable between all groups and similar to the values reported in previous studies [19,20].

9.2 Absorption Studies with and without Flow in the DynaMiTES

Morphological investigation with and without flow did not result in cell detachment or hole formation in the epithelium. Because we were able to detect injuries close to the margins using SEM imaging, we could also conclude that insertion of our in vitro model into the DynaMiTES did not cause any damage. This assumption was

https://doi.org/10.24355/dbbs.084-201904011253-0

supported by other previous results. Extensive detachment of the cells would have decreased the obtained cell viability as previously demonstrated for stromal equivalents (see Figure 4 and Figure 7). Moreover, regardless of flow exposure, no significant decrease in TEER or increase in P_{app} values occurred in the DynaMiTES. Thus, no negative effects of the flow were expected. Nevertheless, the flow rates of the current study were relatively low. Consequently, the shear stresses (1.72×10^{-4} Pa for 148 µL/min; for shear stress calculation see PART 1) were much lower compared to the in vivo conditions (up to 15 Pa [15]). However, we only aimed to simulate tear drainage and thus did not intend to apply shear stress similar to physiological blinking forces. In the present work, the shear stresses and short exposure time resulted in slight changes in cell morphology or TEER, which might be extended with application of higher shear stresses and a prolongation of flow exposure. Stimulating or life extending effects of physiological flow have for example been reported for models of the human gut [25], liver and skin [50,55]. Regarding monolayers of SV-40 immortalized corneal epithelial cell lines, Pretor et al. found no morphological changes with a shear stress of 0.1 Pa [38]. However, Utsunomiya et al. observed significantly decrease in wound healing and corneal cell proliferation after the exposition to 1.2 Pa [48]. For this reason, an effect of increased shear stress in drug absorption testing or specifically in dynamic cultivation for the inverted HC (see Section 10) should be further investigated in subsequent studies.

In addition to the investigation of flow effects, we showed the reliability and benefit of the inbuilt TEER electrodes in real-time TEER assessment. Because standard measuring systems, such as EVOM2 combined with EndOhm® Chamber, only allow TEER analysis before and after the absorption study without any disruption, no real-

https://doi.org/10.24355/dbbs.084-201904011253-0

time information with a time-dependent evaluation of substance barrier interactions is feasible. Alternative measurement systems, such as the EVOM2 with chopstick electrode (STX2 electrode, WPI, Sarasota, Florida, US), entail multiple error possibilities as variable electrode positions and cross-contamination of the tested substance. Fortunately, our DynaMiTES resolves all these challenges and enhances the informational content that is obtained in in vitro absorption studies.

9.3 Dynamic Permeation Studies in the DynaMiTES

In our first dynamic experiments without BAC, the novel and in vivo-like test procedure showed a reduced concentration profile compared to static conditions. This finding resulted from shorter exposure time periods to sodium fluorescein in consequence of the simulated tear drainage. Moreover, the dynamic curve flattened over the permeation time due to of the diminishing concentration in the donor compartment and the consequently decreasing concentration gradient. This progression more resembled the physiological kinetics [13,42] than static conditions. In the latter, the high donor concentration generated a constant concentration gradient during the entire experimental time. As a result, higher acceptor concentrations and linear concentration-time curves were achieved under static conditions. Although, these findings enable further calculation of the P_{app} as a parameter for substance absorption, this profile progression cannot be easily transferred to in vivo conditions [46].

Apart from the differences in static and dynamic experimental conditions, we investigated the effect of BAC. Because this substance is a common and frequently used preservative, many studies examining the effects of BAC have been previously performed. Among these studies, an increasing harmful potential with increasing concentration has been reported [11,18,36] and was also found in the present study.

https://doi.org/10.24355/dbbs.084-201904011253-0

For example, the lowest BAC concentration (0.005 %) showed neither an effect under static nor under dynamic conditions. The doubled concentration then caused a clear effect only under static conditions (4.3-fold increase in P_{app}), which could be marginally increased with a higher BAC concentration. For 0.02 % BAC, the P_{app} was 4.5-fold higher than the reference without BAC. In this case, the non-physiological static exposure time of 30 min may have resulted in an immense and maximum barrier-impairing effect for 0.01 % and 0.02 % BAC. Consequently, no further increase in permeability was observed with increasing concentration. Moreover, this large barrier disruption may have caused a dramatic reduction in lag time for sodium fluorescein permeation under these conditions.

However, no increase in sodium fluorescein concentration was found for dynamic conditions lower than 0.02 % BAC. This high concentration then caused a 10.3-fold increase in acceptor concentration compared to dynamic conditions without BAC. No effect was found below 0.02 % BAC, which was consistent with findings obtained in the study performed by Burstein [8], who investigated sodium fluorescein permeability in vivo (dynamic conditions). In their study, 0.01 % BAC also showed no significant increase. However, the permeability was increased 1.23-fold by 0.02 % of BAC. The effect of 0.02 % BAC was also investigated by Uematsu et al. [47] using an in vivo TEER measuring system. A significant decrease in TEER was observed in humans at 0.02% BAC but not at 0.01 % BAC. Higher concentrations were not tested due to their harmful potential [17]. Furthermore, both studies showed, that both investigated rabbit groups were more susceptible to BAC and yielded significant results at lower concentrations compared to humans [8,47]. These findings underline once more that rabbits cannot reliably predict human physiology and that alternative test systems are needed.

https://doi.org/10.24355/dbbs.084-201904011253-0

570 Apart from concentration-dependent effects, exposure time-dependent effects have
571 also been reported for BAC [18,29,46]. For example, Nakagawa et al. [34] found no
572 significant increase in carboxyfluorescein permeability for 0.002 % BAC after 10 min
573 exposure, but only after 6 h exposure. These investigations highlight that the results
574 are not only dependent on the BAC concentration but also on its exposure time. In
575 our experiments, 0.01 % BAC significantly increased the concentration curve under
576 static conditions but not under dynamic conditions, as the exposure time was clearly
577 shorter and in vivo-like in the dynamic test system.

578 Because BAC is rapidly diluted in vivo [16], dynamic test conditions have always
579 been favorable but rarely developed. Nakamura et al. [35] generated a dynamic ex
580 vivo test system in which the rabbit cornea is mounted in an Ussing chamber system
581 and the donor compartment is drained by a peristaltic pump. Similar to the previously
582 described studies, the decrease in TEER was higher with increasing BAC
583 concentration. More importantly, the turnover rate was varied to simulate normal or
584 dry eye precorneal physiology, and an increasing harmful potential with decreasing
585 flow rate was observed. These findings were confirmed by our results, as we were
586 able to nearly eliminate the barrier-impairing effect of 0.02 % BAC with an elevated
587 flow rate (10.3-fold vs. 1.6-fold increase of sodium fluorescein concentration). The
588 importance of the chosen flow rate may also explain the relatively high increase in
589 acceptor concentration after dynamic exposure to 0.02 % BAC for the normal flow
590 rate. In our study, the experimental conditions resulted in a 10.3-fold increase.
591 However, Burstein only found a 1.23-fold increase in vivo [8]. Taking this study into
592 consideration, our elevated flow rate resulted in similar values compared to the in
593 vivo conditions, and a better in vivo correlation may be obtained with a slightly higher
594 flow rate. In the study of Nakamura et al. [35], a higher tear flow was selected in

https://doi.org/10.24355/dbbs.084-201904011253-0

595 contrast to our values. However, previous literature reports have described many
596 different physiological flow rates which were mostly investigated using very different
597 methods [1,12,14,33,43]. Thus, additional research studies are needed to determine
598 the optimal conditions to reliably predict in vivo results. Nevertheless, both studies
599 emphasize, the importance of flow rate selection and moreover highlight the great
600 opportunity of controlling the dilution rate, thereby simulating different physiological
601 states.

602 10 Conclusions

603 Overall, the present study showed that adaption of our HC construct to the
604 DynaMiTES was feasible and could be successfully performed. Thus, we propose
605 that other in vitro models may also be adapted and applied using our novel platform.
606 In this way, a future combination of different single DynaMiTES “organs” as proposed
607 in our first study (see PART 1) is implementable.

608 Furthermore, the first dynamic experiments emphasize that the *Ocular* DynaMiTES
609 provides novel and improved information: First, the inbuilt electrodes ensure the real-
610 time assessment of substance barrier interaction. Second, the dynamic donor control
611 enables the simulation of physiological conditions, which may even be varied to
612 emulate healthy or diseased states. Furthermore, our system also showed that static
613 test procedures may be suitable for the evaluation of tissue permeability using P_{app},
614 but not for reliable formulation testing. The DynaMiTES, with its highly controlled
615 dynamic test conditions, showed better correlation with published in vivo data than
616 static conditions. Unfortunately, human corneas are invariably needed for
617 transplantation and are rarely available for other applications, such as in studies
618 using the Ussing chamber system developed by Nakamura et al. For this reason, we

https://doi.org/10.24355/dbbs.084-201904011253-0

619 are convinced that our DynaMiTES represents the optimal combination of a
620 prevalidated human in vitro model and a highly controlled dynamic modular device.
621 With its application in pharmaceutical substance testing, the disadvantages of animal
622 tissue-based test systems and static in vitro models may be circumvented. Finally,
623 automation, which is highly demanded in routine application, is realizable. The donor
624 application has been previously performed using programmable syringe pumps, and
625 the sampling points are provided with septa to enable automatic sampling similar to
626 HPLC autosamplers.

627 Taken together, these advances ease the application in pharmaceutical research and
628 development (R&D). Possible and meaningful applications not only include use in
629 drug absorption but also in functional tests of additives, including permeation
630 enhancers and colloidal systems, such as micelles, liposomes and nanoparticles. In
631 all these areas, dynamic test procedures might generate more reliable findings than
632 non-physiological static test conditions. For this reason, the DynaMiTES is an
633 important contribution to pharmaceutical substance testing and may reduce the
634 prevailing risk of late stage drug failures.

635 In addition to the easy adaption of the HC, the concomitant separation of the
636 epithelium and stroma will enable a more precise investigation of substance
637 absorption than previously feasible with the classic HC. By the PC membrane
638 division, it is conceivable that substance accumulation in the two cell compartments
639 can be investigated independently within or after the experiment. In this way, more
640 pharmacokinetic information of the drug absorption can be obtained.

641 Nevertheless, further improvements of the *Ocular* DynaMiTES will focus on the
642 implementation of online analysis of the acceptor concentration via an inbuilt sensor.
643 Unfortunately, online sensors for this use would require high sensitivity. Thus,

https://doi.org/10.24355/dbbs.084-201904011253-0

external analysis must be maintained until sufficient technology becomes available. Another technical improvement would be downsizing the compartments to reduce the required substance amount. This is specifically desirable in the preclinical phases when few drug is assessable. However, effects of substance distribution and elimination by tear flow would be more in vivo-like if the volume of the compartments is reduced.

Considering the cellular aspects, an investigation of different flow profiles may enhance the comprehension of ocular drug absorption. Furthermore, dynamic cultivation and its effect on the epithelial barrier should be examined. Taken together, these technical and cellular improvements may provide a correlation of the in vitro results with clinical findings. In summary, the present study underlines the particular value of our novel DynaMiTES system and our successful aim to raise the prevalidated HC to a new sustainable level in in vitro drug absorption testing.

11 Acknowledgements

The author NB was funded by the Niedersächsisches Ministerium für Wissenschaft und Kultur (MWK) in the joint project SynFoBiA – “Novel synthesis and formulation methods for poorly soluble drugs and sensitive biopharmaceuticals” and the author KM by the Graduate Program µ-Props – “Processing of Poorly Soluble Drugs at Small Scale” within the scope of the Center of Pharmaceutical Engineering (PVZ) of the TU Braunschweig.

The authors wish to thank Dr. M. Zorn-Kruppa (Hamburg, Germany) and Dr. K. Araki-Sasaki (Kagoshima Japan) for their generous gifts of the HCK and HCE-T cell lines. Furthermore, we would like to express our gratitude to Ulrike Kruse for her technical assistance in cell culture and histology.

https://doi.org/10.24355/dbbs.084-201904011253-0

12 Captions

Figure 1: Images of the DynaMiTES; A: The assembled DynaMiTES; B: The three separate levels (from left to right): top level, insert level and bottom level.

Figure 2: Depiction of the experimental setup for donor flow or donor dilution experiments; sodium fluorescein donor (yellow) was pumped through the DynaMiTES by applying different flow rates. The permeated amount was measured in the acceptor (light blue). For a clearer overview the incubator is not shown, however, all experiments were performed at 37 °C.

Figure 3: Comparison of classic (left; following [20]) and inverted (right) cultivation; light microscopic images show the multilayered epithelium at day 10 of cultivation, which was induced by air-liquid interface (ALI).

Figure 4: Cell viability assessed by MTT dye reaction of classic hemicorneas, inverted hemicorneas and stroma equivalents (without HCE-T cells) at day 10 of cultivation; classic hemicorneas were set to 100 % (mean ± SD.; n = 7-10; ** $p < 0.01$).

Figure 5: TEER profiles of classic and inverted hemicorneas from day 6 to day 13 of cultivation; air-liquid interface cultivation from day 7 on is marked by a light-blue frame (mean ± SD; n = 3-8; ** $p < 0.01$).

Figure 6: Comparative permeation study of classic and inverted hemicornea (HC); A: Experimental setup for classic (top) and inverted (bottom) HC with sodium fluorescein donor solution (yellow) and KRB acceptor solution (light blue); yellow arrows mark the direction of sodium fluorescein permeation; B: Resulting apparent

https://doi.org/10.24355/dbbs.084-201904011253-0

690 permeation coefficient of sodium fluorescein for classic and inverted HC compared to
691 Hahne et al. [20] (mean ± SD; n = 6-7).

692 Figure 7: Cell viability determined by MTT dye reaction after 180 min with and without
693 flow exposition; the negative control (KRB) was kept in a standard well plate and set
694 to 100 %. The samples of 0 µL/min were inserted into the DynaMiTES and the
695 system was filled only once (mean ± SD; n = 4-16; ** $p < 0.01$).

696 Figure 8: Relative TEER profiles obtained over the course of 180 min with and
697 without flow; the negative control was kept in a standard well plate (0 µL/min well
698 plate). The samples for the rate of 0 µL/min were inserted into the DynaMiTES and
699 the system was filled only once. All groups in the DynaMiTES (except 73 µL/min) are
700 significantly different ($p < 0.05$) to the negative control after 180 min but not to the
701 reference in the DynaMiTES (0 µL/min DynaMiTES). For a clearer overview symbols
702 for significant differences are not shown (mean ± SD; n = 4-57).

703 Figure 9: Permeation coefficient of sodium fluorescein with and without different flow
704 rates; 0 µL/min in the well plate served as a negative control and 0.01 % BAC served
705 as a positive control (mean ± SD; n = 6-46; ** significantly different to all other
706 groups, $p < 0.01$).

707 Figure 10: Acceptor concentration of sodium fluorescein over the course of 180 min;
708 A: comparison of common static and innovative dynamic conditions each with and
709 without benzalkonium chloride (BAC) utilizing the DynaMiTES; B: enlarged view of
710 the lower permeation profiles of A (mean ± SD; n = 2-6).

711 Table 1: Cell morphology of inverted human hemicornea at day 10 of cultivation with
712 1 h, 3 h or 18 h (overnight) epithelial cell attachment during fabrication; “hair-like”

https://doi.org/10.24355/dbbs.084-201904011253-0

structures in the epithelium resulted from the known but unavoidable interaction of the PC membrane and resin material.

Table 2: Images of light microscopy (left) and scanning electron microscopy (right) of inverted hemicorneas after 180 min with and without flow; the negative control was kept in a standard well plate (0 µL/min well plate). The samples of 0 µL/min were inserted into the DynaMiTES and the system was filled only once (0 µL/min DynaMiTES). For the positive control, inverted HCs were scratched with a glass pipette. The injured area with the visible PC membrane is marked in red.

13 References

[1] American Academy of Ophthalmology, Fundamentals and Principles of Ophthalmology: Part 3: Biochemistry and Metabolism, American Academy of Ophthalmology, 1989.

[2] K. Araki-Sasaki, Y. Ohashi, T. Sasabe, K. Hayashi, H. Watanabe, Y. Tano, H. Handa, An SV40-immortalized human corneal epithelial cell line and its characterization, Investigative Ophthalmology and Visual Science 36 (1995) 614–621.

[3] B. Ataç, I. Wagner, R. Horland, R. Lauster, U. Marx, A.G. Tonevitsky, R.P. Azar, G. Lindner, Skin and hair on-a-chip: In vitro skin models versus ex vivo tissue maintenance with dynamic perfusion, Lab on a Chip - Miniaturisation for Chemistry and Biology 13 (2013) 3555–3561.

[4] J. Barar, A.R. Javadzadeh, Y. Omidi, Ocular novel drug delivery: Impacts of membranes and barriers, Expert Opinion on Drug Delivery 5 (2008) 567–581.

https://doi.org/10.24355/dbbs.084-201904011253-0

[5] N. Beißner, T. Lorenz, S. Reichl, Organ on Chip, in: A. Dietzel (Ed.), Microsystems for Pharmatechnology: Manipulation of Fluids, Particles, Droplets, and Cells, 1st ed., Springer, 2016, pp. 299–339.

[6] R. Booth, H. Kim, Characterization of a microfluidic in vitro model of the blood-brain barrier (μBBB), Lab on a Chip - Miniaturisation for Chemistry and Biology 12 (2012) 1784–1792.

[7] M. Bur, B. Rothen-Rutishauser, H. Huwer, C.-M. Lehr, A novel cell compatible impingement system to study in vitro drug absorption from dry powder aerosol formulations, European Journal of Pharmaceutics and Biopharmaceutics 72 (2009) 350–357.

[8] N.L. Burstein, Preservative alteration of corneal permeability in humans and rabbits, Investigative ophthalmology & visual science 25 (1984) 1453.

[9] O. Camber, P. Edman, Influence of some preservatives on the corneal permeability of pilocarpine and dexamethasone, in vitro, International Journal of Pharmaceutics 39 (1987) 229–234.

[10] A.K. Capulli, K. Tian, N. Mehandru, A. Bukhta, S.F. Choudhury, M. Suchyta, K.K. Parker, Approaching the in vitro clinical trial: Engineering organs on chips, Lab on a Chip - Miniaturisation for Chemistry and Biology 14 (2014) 3181–3186.

[11] W. Chen, Z. Li, J. Hu, Z. Zhang, L. Chen, Y. Chen, Z. Liu, Corneal alternations induced by topical application of benzalkonium chloride in rabbit, PLoS ONE 6 (2011).

[12] C. Chow, J.P. Gilbard, Tear Film, in: J.H. Krachmer, M.J. Mannis, E.J. Holland (Eds.), Cornea: Fundamentals of Cornea and External Disease, 1st ed., Mosby, St. Louis, Mo., 1997, pp. 49–60.

https://doi.org/10.24355/dbbs.084-201904011253-0

759 [13] S.S. Chrai, T.F. Patton, A. Mehta, J.R. Robinson, Lacrimal and instilled fluid
760 dynamics in rabbit eyes, Journal of Pharmaceutical Sciences 62 (1973) 1112–
761 1121.
762 [14] J.P. Craig, A. Tomlison, L. McCann, Tear Film, in: D.A. Dartt (Ed.),
763 Encyclopedia of the eye, Elsevier Acad. Press, Amsterdam, 2010, pp. 254–262.
764 [15] P.N. Dilly, Structure and function of the tear film, in: D.A. Sullivan (Ed.),
765 Lacrimal Gland, Tear Film and Dry Eye Syndroms: Basic Science and Clinical
766 Relevance, Plenum Press, New York and London, 1994, pp. 239–247.
767 [16] M.H. Friedlaender, D. Breshears, H. Sheardown, B. Amoozgar, M. Senchyna,
768 The dilution of benzalkonium chloride (BAK) in the tear film, Advances in Therapy
769 23 (2006) 835–841.
770 [17] K. Green, The effects of preservatives on corneal permeability of drugs, in: P.
771 Edman (Ed.), Biopharmaceutics of ocular drug delivery, CRC Press, Boca Raton,
772 Fla, 1993, pp. 43–59.
773 [18] K. Green, A.M. Tonjum, The effect of benzalkonium chloride on the
774 electropotential of the rabbit cornea, Acta Ophthalmologica 53 (1975) 348–357.
775 [19] M. Hahne, S. Reichl, Development of a serum-free human cornea construct
776 for in vitro drug absorption studies: The influence of varying cultivation parameters
777 on barrier characteristics, International Journal of Pharmaceutics 416 (2011) 268–
778 279.
779 [20] M. Hahne, M. Zorn-Kruppa, G. Guzman, J.M. Brandner, E. Haltner-Ukomado,
780 H. Wätzig, S. Reichl, Prevalidation of a human cornea construct as an alternative
781 to animal corneas for in vitro drug absorption studies, Journal of Pharmaceutical
782 Sciences 101 (2012) 2976–2988.
783 [21] M. Hornof, E. Toropainen, A. Urtti, Cell culture models of the ocular barriers,
784 Eur. J. Pharm. Biopharm. 60 (2005) 207–225.

https://doi.org/10.24355/dbbs.084-201904011253-0

785 [22] D. Huh, B.D. Matthews, A. Mammoto, M. Montoya-Zavala, H. Yuan Hsin, D.E.
786 Ingber, Reconstituting organ-level lung functions on a chip, Science 328 (2010)
787 1662–1668.
788 [23] K. Järvinen, T. Järvinen, A. Urtti, Ocular absorption following topical delivery,
789 Advanced Drug Delivery Reviews 16 (1995) 3–19.
790 [24] I.P. Kaur, R. Smitha, Penetration Enhancers and Ocular Bioadhesives: Two
791 New Avenues for Ophthalmic Drug Delivery, Drug Development and Industrial
792 Pharmacy 28 (2002) 353–369.
793 [25] H.J. Kim, D. Huh, G. Hamilton, D.E. Ingber, Human gut-on-a-chip inhabited by
794 microbial flora that experiences intestinal peristalsis-like motions and flow, Lab on
795 a Chip - Miniaturisation for Chemistry and Biology 12 (2012) 2165–2174.
796 [26] Kirkstall Ltd., homepage, http://kirkstall.org/index.php/quasi-vivo-products/,
797 accessed 14 December 2016.
798 [27] C. Kölln, S. Reichl, Cytochrome P450 Activity in Ex Vivo Cornea Models and a
799 Human Cornea Construct, Journal of Pharmaceutical Sciences 105 (2016) 2204–
800 2212.
801 [28] C. Kölln, S. Reichl, Expression of glutathione transferases in corneal cell lines,
802 corneal tissues and a human cornea construct, International Journal of
803 Pharmaceutics 506 (2016) 371–381.
804 [29] M. Kusano, M. Uematsu, T. Kumagami, H. Sasaki, T. Kitaoka, Evaluation of
805 acute corneal barrier change induced by topically applied preservatives using
806 corneal transepithelial electric resistance in vivo, Cornea 29 (2010) 80–85.
807 [30] L. Maciuleviciute, C. Hornberg, N.H. Seemayer, Rodent tracheal epithelial
808 cells in vitro: A comparative study of normal cells, enhanced growth variants, SV-
809 40 transformed cells and their interactions, Toxicology Letters 88 (1996) 55–64.

https://doi.org/10.24355/dbbs.084-201904011253-0

[31] S. Maher, L. Feighery, D.J. Brayden, S. McClean, Melittin as a permeability enhancer II: in vitro investigations in human mucus secreting intestinal monolayers and rat colonic mucosae, Pharmaceutical Research 24 (2007) 1346–1356.

[32] U. Marx, H. Walles, S. Hoffmann, G. Lindner, R. Horland, F. Sonntag, U. Klotzbach, D. Sakharov, A. Tonevitsky, R. Lauster, 'Human-on-a-chip' developments: A translational cuttingedge alternative to systemic safety assessment and efficiency evaluation of substances in laboratory animals and man?, ATLA Alternatives to Laboratory Animals 40 (2012) 235–257.

[33] S. Mishima, A. Gasset, S.D. Klyce, Baum, J. L. [JR.], Determination of tear volume and tear flow, Investigative ophthalmology 5 (1966) 264–276.

[34] S. Nakagawa, T. Usui, S. Yokoo, S. Omichi, M. Kimakura, Y. Mori, K. Miyata, M. Aihara, S. Amano, M. Araie, Toxicity evaluation of antiglaucoma drugs using stratified human cultivated corneal epithelial sheets, Investigative Ophthalmology and Visual Science 53 (2012) 5154–5160.

[35] T. Nakamura, M. Teshima, T. Kitahara, H. Sasaki, M. Uematsu, T. Kitaoka, M. Nakashima, K. Nishida, J. Nakamura, S. Higuchi, Sensitive and real-time method for evaluating corneal barrier considering tear flow, Biological and Pharmaceutical Bulletin 33 (2010) 107–110.

[36] T. Nakamura, M. Yamada, M. Teshima, M. Nakashima, H. To, N. Ichikawa, H. Sasaki, Electrophysiological characterization of tight junctional pathway of rabbit cornea treated with ophthalmic ingredients, Biological and Pharmaceutical Bulletin 30 (2007) 2360–2364.

[37] I. Pepić, J. Lovrić, B. Cetina-Čižmek, S. Reichl, J. Filipović-Grčić, Toward the practical implementation of eye-related bioavailability prediction models, Drug Discovery Today 19 (2014) 31–44.

https://doi.org/10.24355/dbbs.084-201904011253-0

836 [38] S. Pretor, J. Bartels, T. Lorenz, K. Dahl, J.H. Finke, G. Peterat, R. Krull, A.T.
837 Al-Halhouli, A. Dietzel, S. Büttgenbach, S. Reichl, C.C. Müller-Goymann, Cellular
838 uptake of coumarin-6 under microfluidic conditions into HCE-T cells from
839 nanoscale formulations, Molecular Pharmaceutics 12 (2015) 34–45.
840 [39] K.J. Regehr, M. Domenech, J.T. Koepsel, K.C. Carver, S.J. Ellison-Zelski,
841 W.L. Murphy, L.A. Schuler, E.T. Alarid, D.J. Beebe, Biological implications of
842 polydimethylsiloxane-based microfluidic cell culture, Lab on a Chip -
843 Miniaturisation for Chemistry and Biology 9 (2009) 2132–2139.
844 [40] S. Reichl, Cell culture models of the human cornea - A comparative evaluation
845 of their usefulness to determine ocular drug absorption in-vitro, Journal of
846 Pharmacy and Pharmacology 60 (2008) 299–307.
847 [41] H. Sasaki, K. Yamamura, C. Tei, K. Nishida, J. Nakamura, Ocular permeability
848 of FITC-dextran with absorption promoter for ocular delivery of peptide drug,
849 Journal of Drug Targeting 3 (1995) 129–135.
850 [42] J.W. Shell, Pharmacokinetics of topically applied ophthalmic drugs, Survey of
851 Ophthalmology 26 (1982) 207–218.
852 [43] T. Sörensen, F. Taagehöj Jensen, Tear flow in normal human eyes.
853 determination by means of radioisotope and gamma camera, Acta
854 Ophthalmologica 57 (1979).
855 [44] G.I. Tennekoon, J. Yoshino, K. Peden, J. Bigbee, J.L. Rutkowski, Y.
856 Kishimoto, G.H. DeVries, G.M. McKhann, Transfection of neonatal rat Schwann
857 cells with SV-40 large T antigen gene under control of the metallothionein
858 promoter, Journal of Cell Biology 105 (1987) 2315–2325.
859 [45] M.W. Toepke, D.J. Beebe, PDMS absorption of small molecules and
860 consequences in microfluidic applications, Lab on a Chip - Miniaturisation for
861 Chemistry and Biology 6 (2006) 1484–1486.

https://doi.org/10.24355/dbbs.084-201904011253-0

862 [46] A.M. Tonjum, Permeability of rabbit corneal epithelium to horseradish
863 peroxidase after the influence of benzalkonium chloride, Acta Ophthalmologica 53
864 (1975) 335–347.
865 [47] M. Uematsu, Y.H. Mohamed, N. Onizuka, R. Ueki, D. Inoue, A. Fujikawa, H.
866 Sasaki, T. Kitaoka, Less Invasive Corneal Transepithelial Electrical Resistance
867 Measurement Method, Ocular Surface 14 (2016) 37–42.
868 [48] T. Utsunomiya, A. Ishibazawa, T. Nagaoka, K. Hanada, H. Yokota, N. Ishii, A.
869 Yoshida, Transforming growth factor-B signaling cascade induced by mechanical
870 stimulation of fluid shear stress in cultured corneal epithelial cells, Investigative
871 Ophthalmology and Visual Science 57 (2016) 6382–6388.
872 [49] M.W. Van Der Helm, A.D. Van Der Meer, Eijkel, J. C. T., A. Van Den Berg, L.I.
873 Segerink, Microfluidic organ-on-chip technology for blood-brain barrier research,
874 Tissue barriers 4 (2016) e1142493.
875 [50] P.M. Van Midwoud, G. Groothuis, M.T. Merema, E. Verpoorte, Microfluidic
876 biochip for the perifusion of precision-cut rat liver slices for metabolism and
877 toxicology studies, Biotechnology and Bioengineering 105 (2010) 184–194.
878 [51] P.M. Van Midwoud, A. Janse, M.T. Merema, G. Groothuis, E. Verpoorte,
879 Comparison of biocompatibility and adsorption properties of different plastics for
880 advanced microfluidic cell and tissue culture models, Analytical Chemistry 84
881 (2012) 3938–3944.
882 [52] J. Verstraelen, S. Reichl, Expression analysis of MDR1, BCRP and MRP3
883 transporter proteins in different in vitro and ex vivo cornea models for drug
884 absorption studies, International Journal of Pharmaceutics 441 (2013) 765–775.
885 [53] J. Verstraelen, S. Reichl, Multidrug resistance-associated protein (MRP1, 2, 4
886 and 5) expression in human corneal cell culture models and animal corneal tissue,
887 Molecular Pharmaceutics 11 (2014) 2160–2171.

https://doi.org/10.24355/dbbs.084-201904011253-0

888 [54] J. Verstraelen, S. Reichl, Upregulation of P-glycoprotein expression by
889 ophthalmic drugs in different corneal in-vitro models, The Journal of pharmacy
890 and pharmacology 67 (2015) 605–615.
891 [55] I. Wagner, E.-M. Materne, S. Brincker, U. Süßbier, C. Frädrich, M. Busek, F.
892 Sonntag, D.A. Sakharov, E.V. Trushkin, A.G. Tonevitsky, R. Lauster, U. Marx, A
893 dynamic multi-organ-chip for long-term cultivation and substance testing proven
894 by 3D human liver and skin tissue co-culture, Lab on a Chip - Miniaturisation for
895 Chemistry and Biology 13 (2013) 3538–3547.
896 [56] Y. Wakabayashi, J. Chua, J.M. Larkin, J. Lippincott-Schwartz, I.M. Arias, Four-
897 dimensional imaging of filter-grown polarized epithelial cells, Histochemistry and
898 Cell Biology 127 (2007) 463–472.
899 [57] M. Zorn-Kruppa, S. Tykhonova, G. Beige, J. Bednarz, H.A. Diehl, M. Engelke,
900 A human corneal equivalent constructed from SV40-immortalised corneal cell
901 lines, Alternatives to Laboratory Animals 33 (2005) 37–45.

https://doi.org/10.24355/dbbs.084-201904011253-0

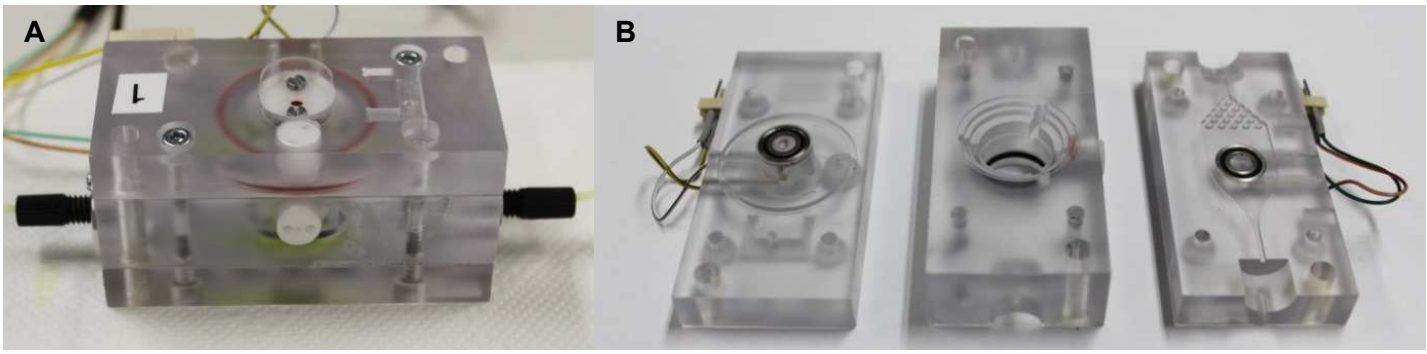

https://doi.org/10.24355/dbbs.084-201904011253-0

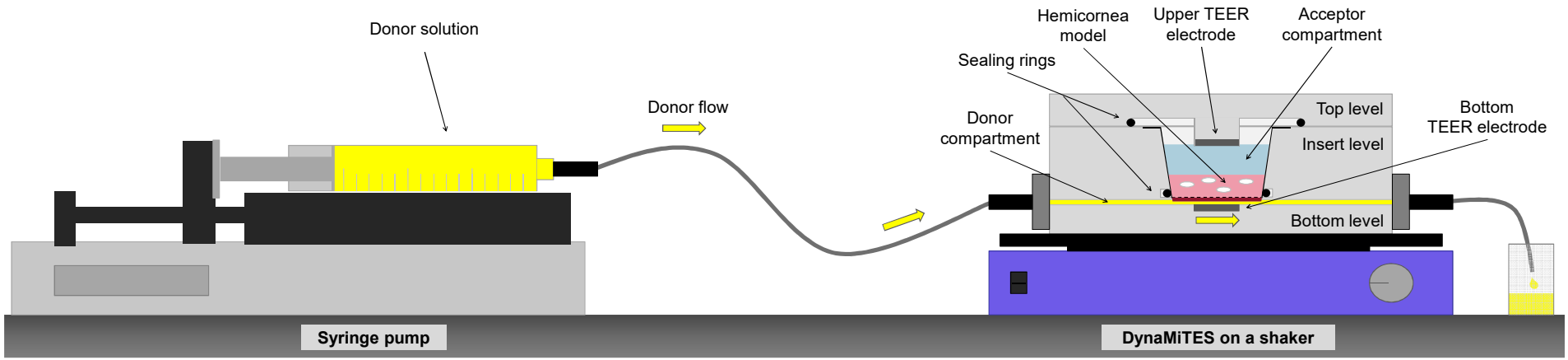

https://doi.org/10.24355/dbbs.084-201904011253-0

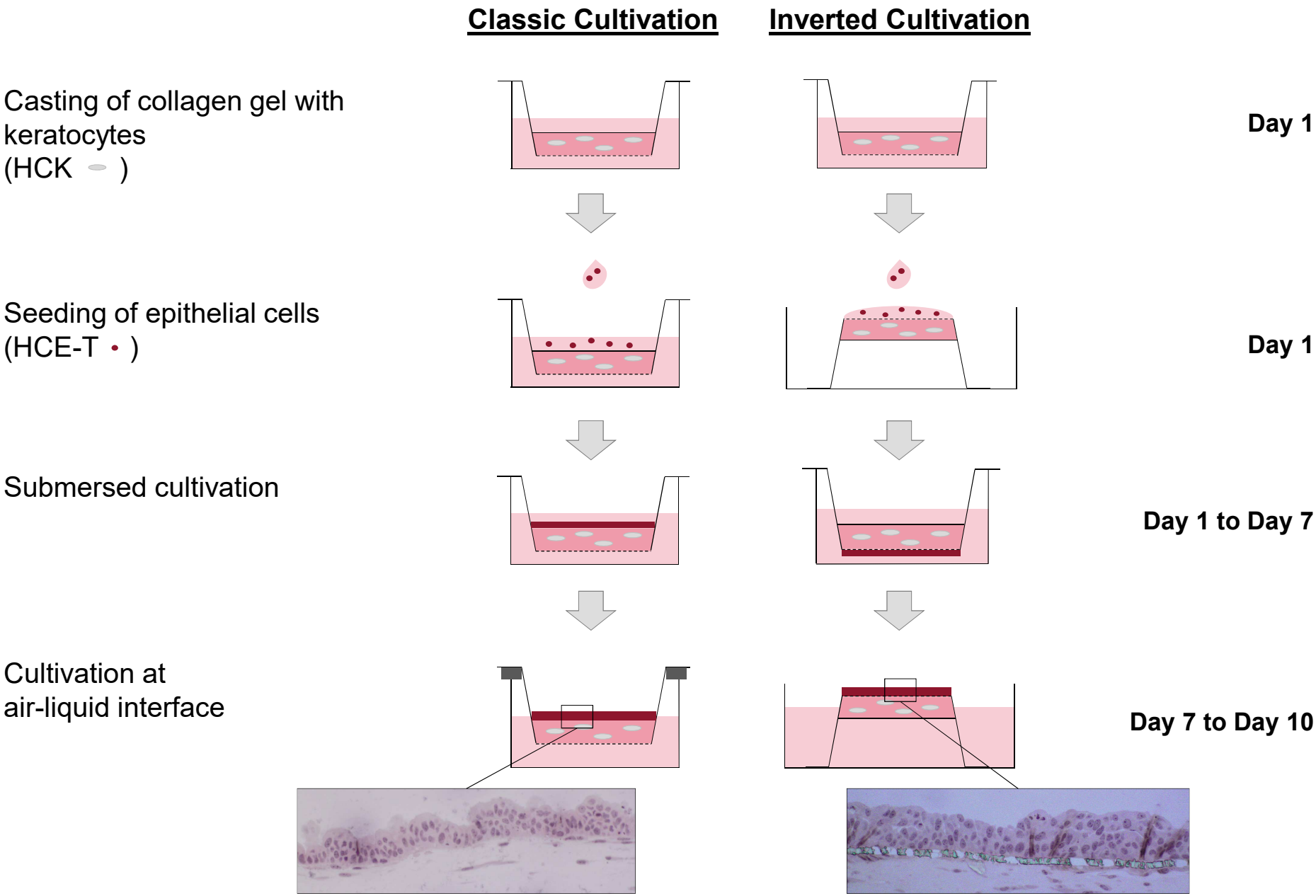

https://doi.org/10.24355/dbbs.084-201904011253-0

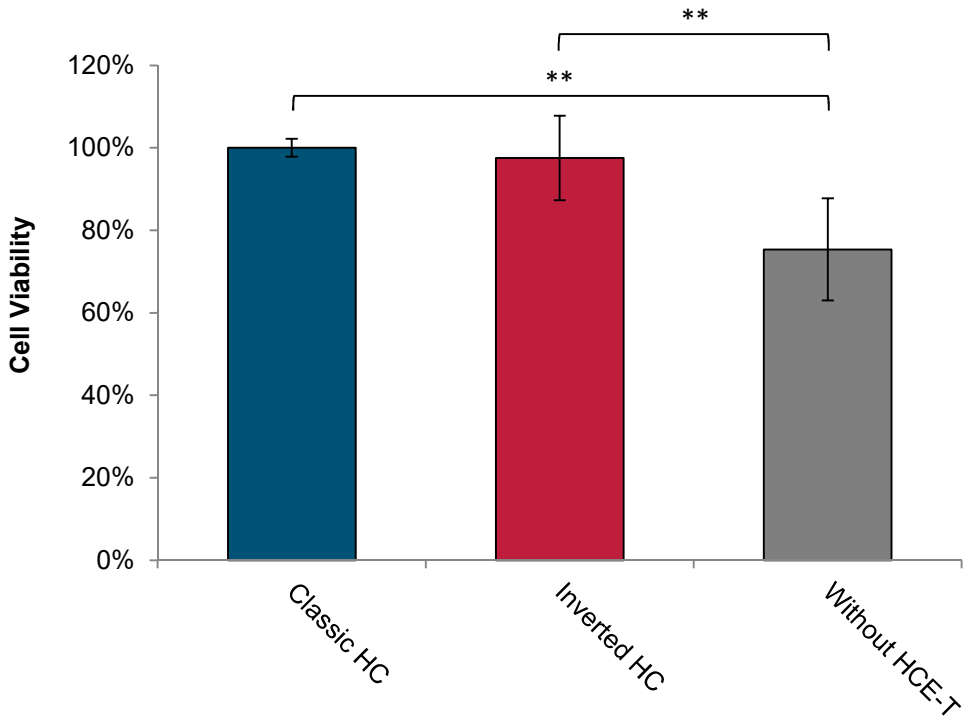

https://doi.org/10.24355/dbbs.084-201904011253-0

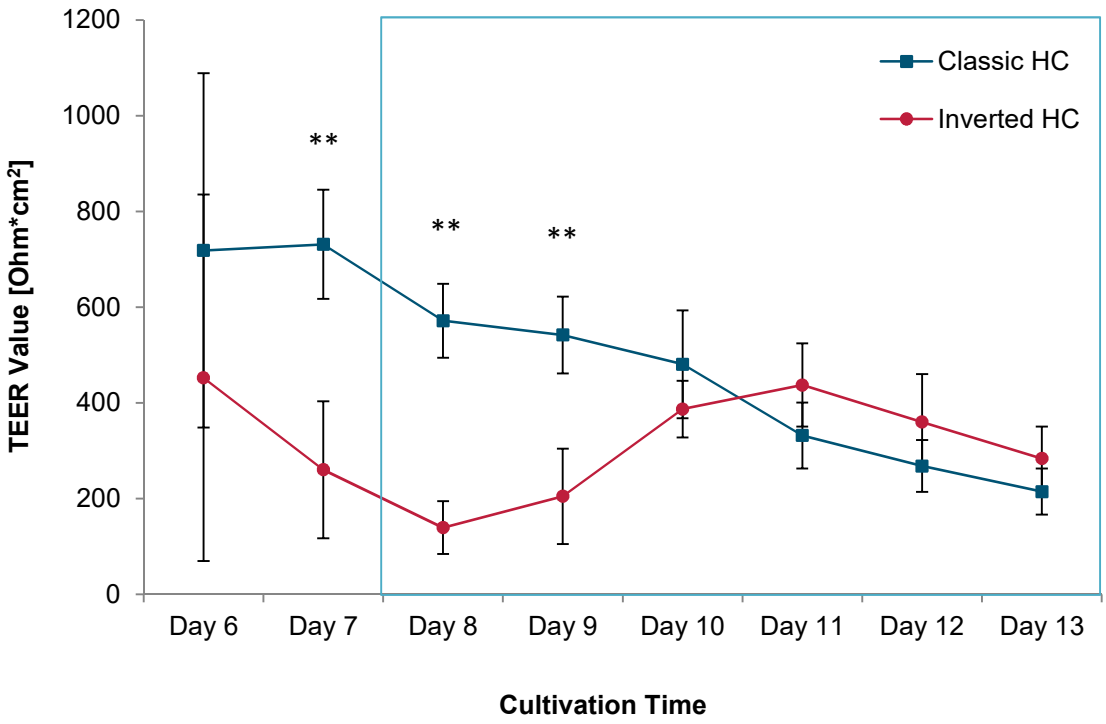

https://doi.org/10.24355/dbbs.084-201904011253-0

A

Classic HC

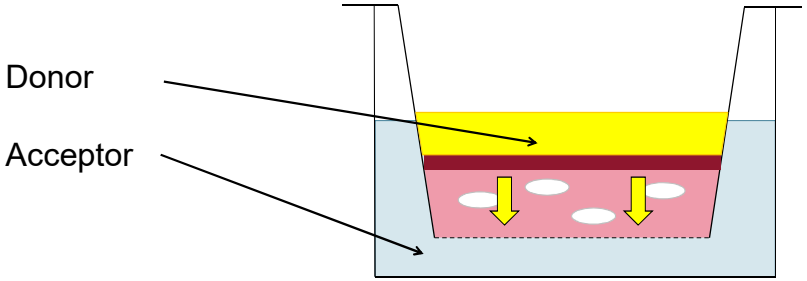

Inverted HC

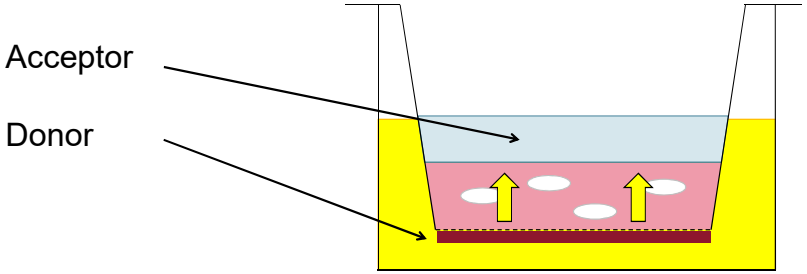

B

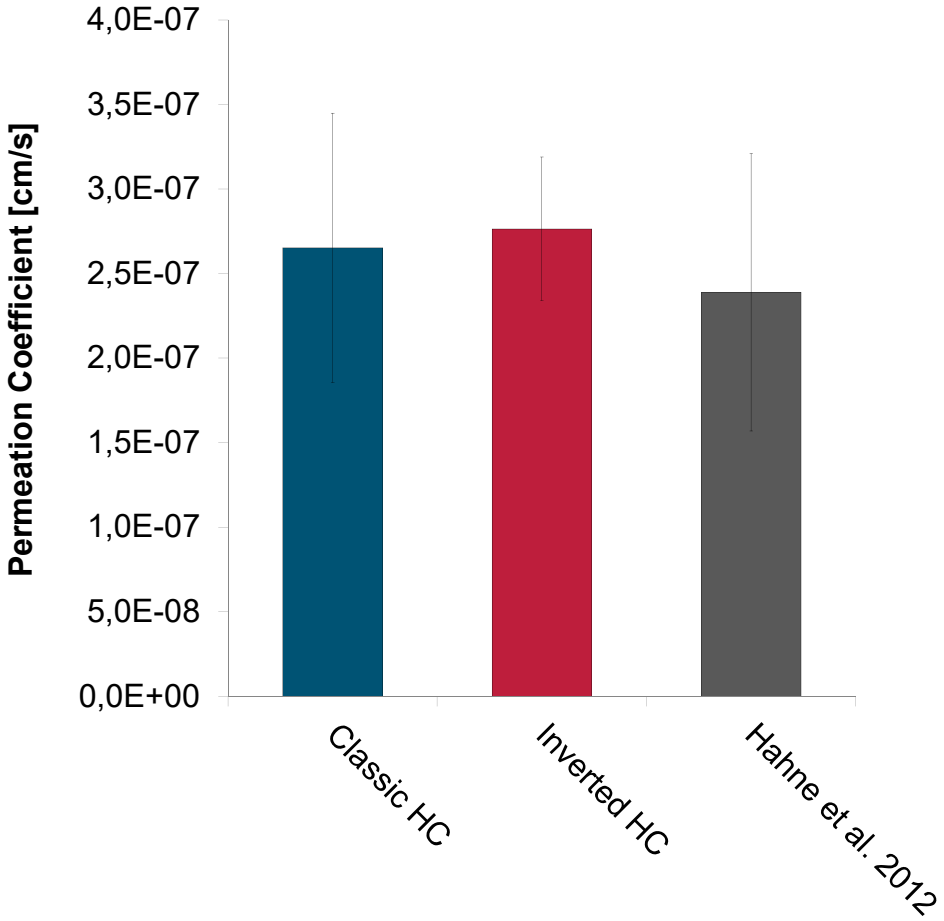

https://doi.org/10.24355/dbbs.084-201904011253-0

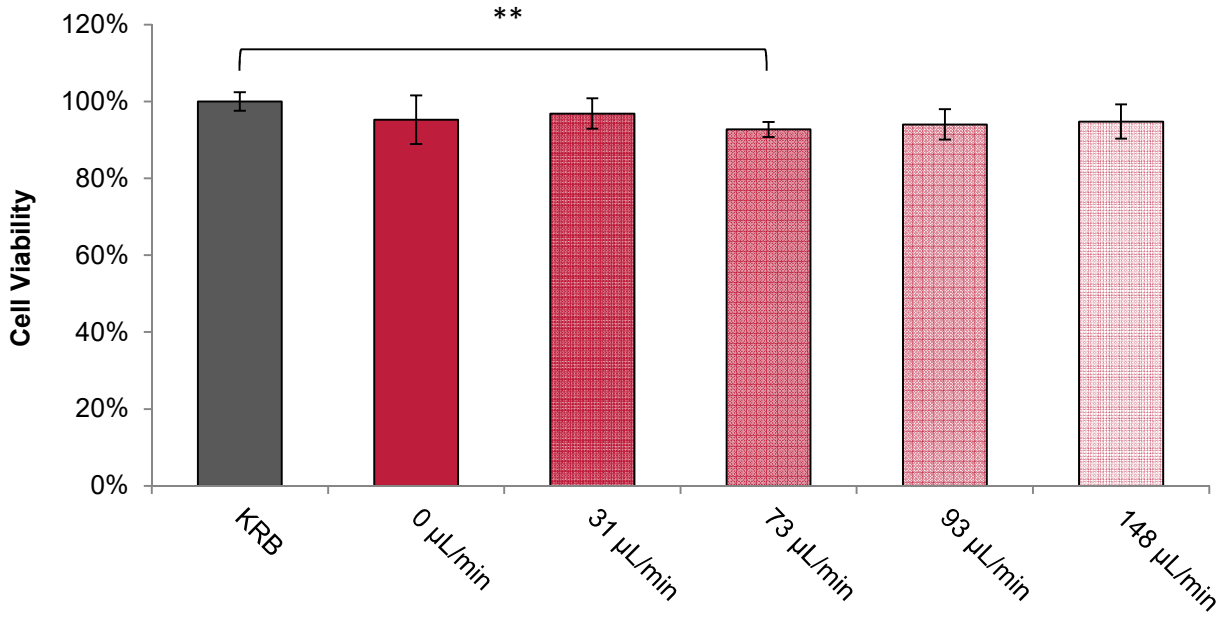

https://doi.org/10.24355/dbbs.084-201904011253-0

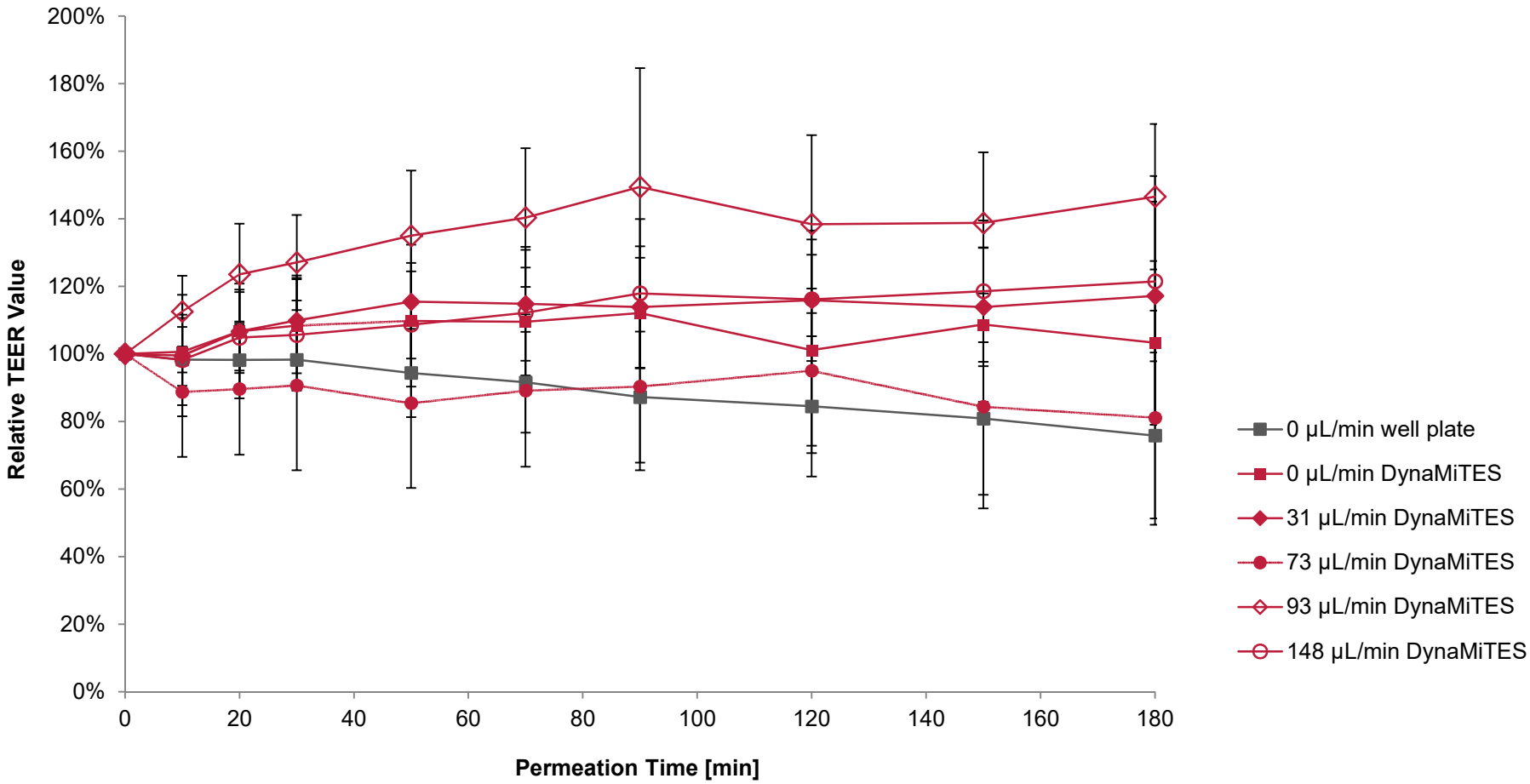

https://doi.org/10.24355/dbbs.084-201904011253-0

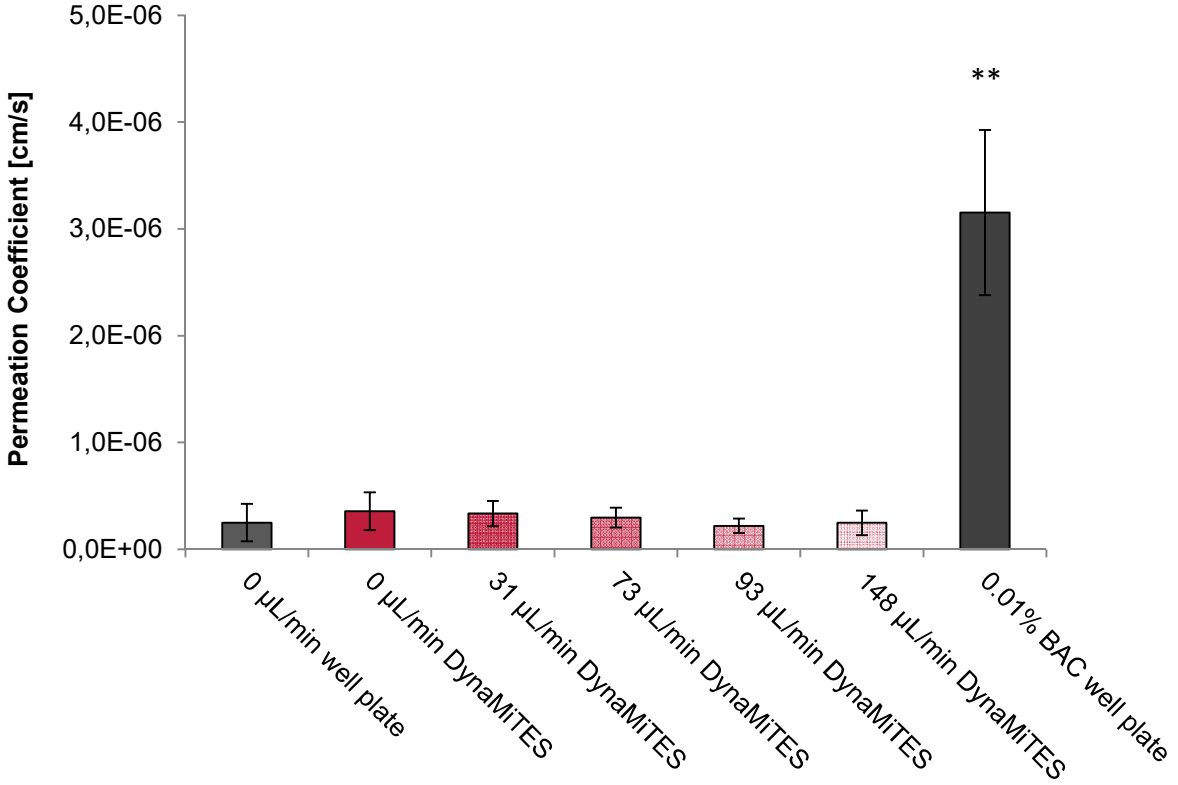

https://doi.org/10.24355/dbbs.084-201904011253-0

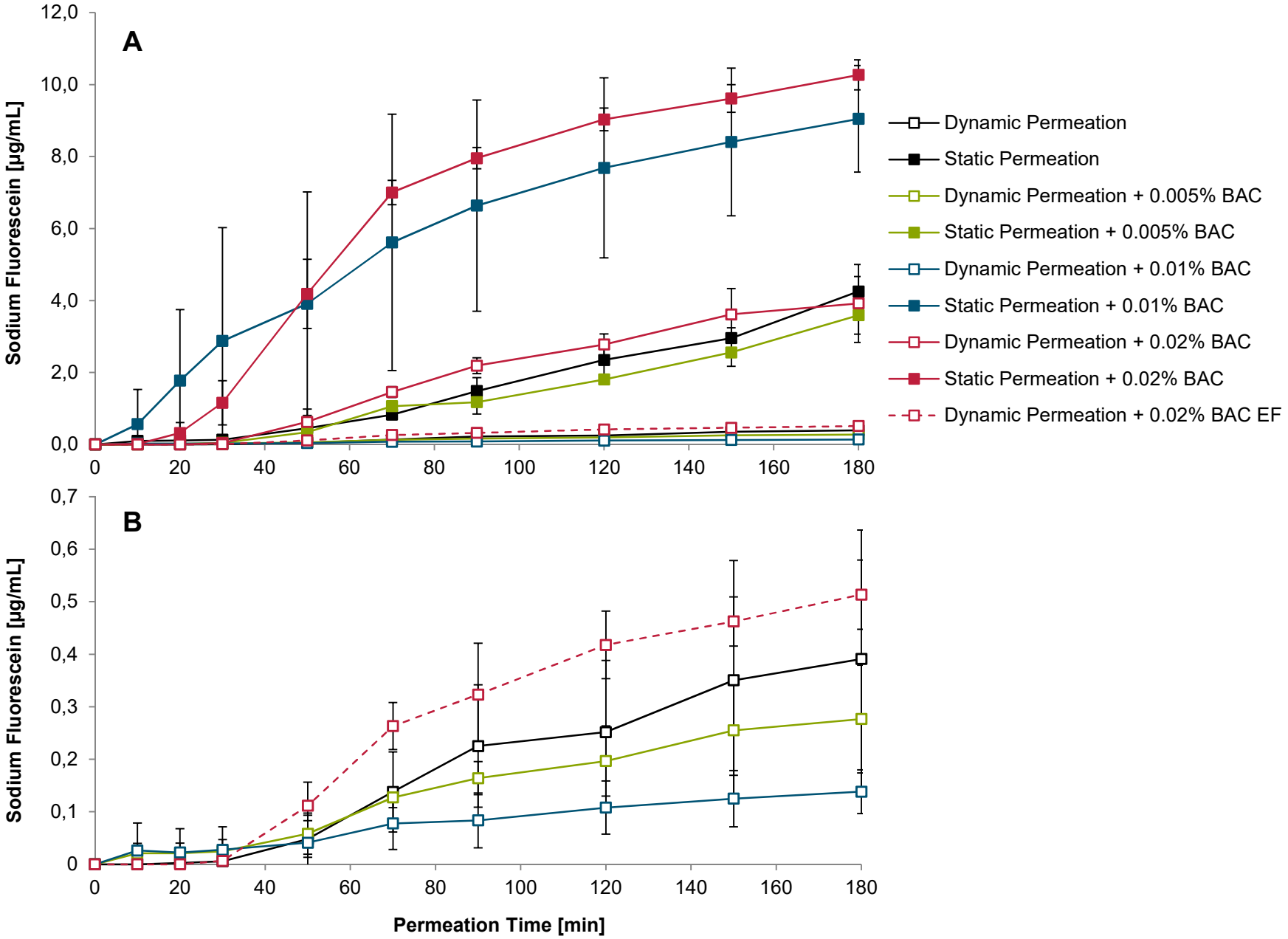

https://doi.org/10.24355/dbbs.084-201904011253-0

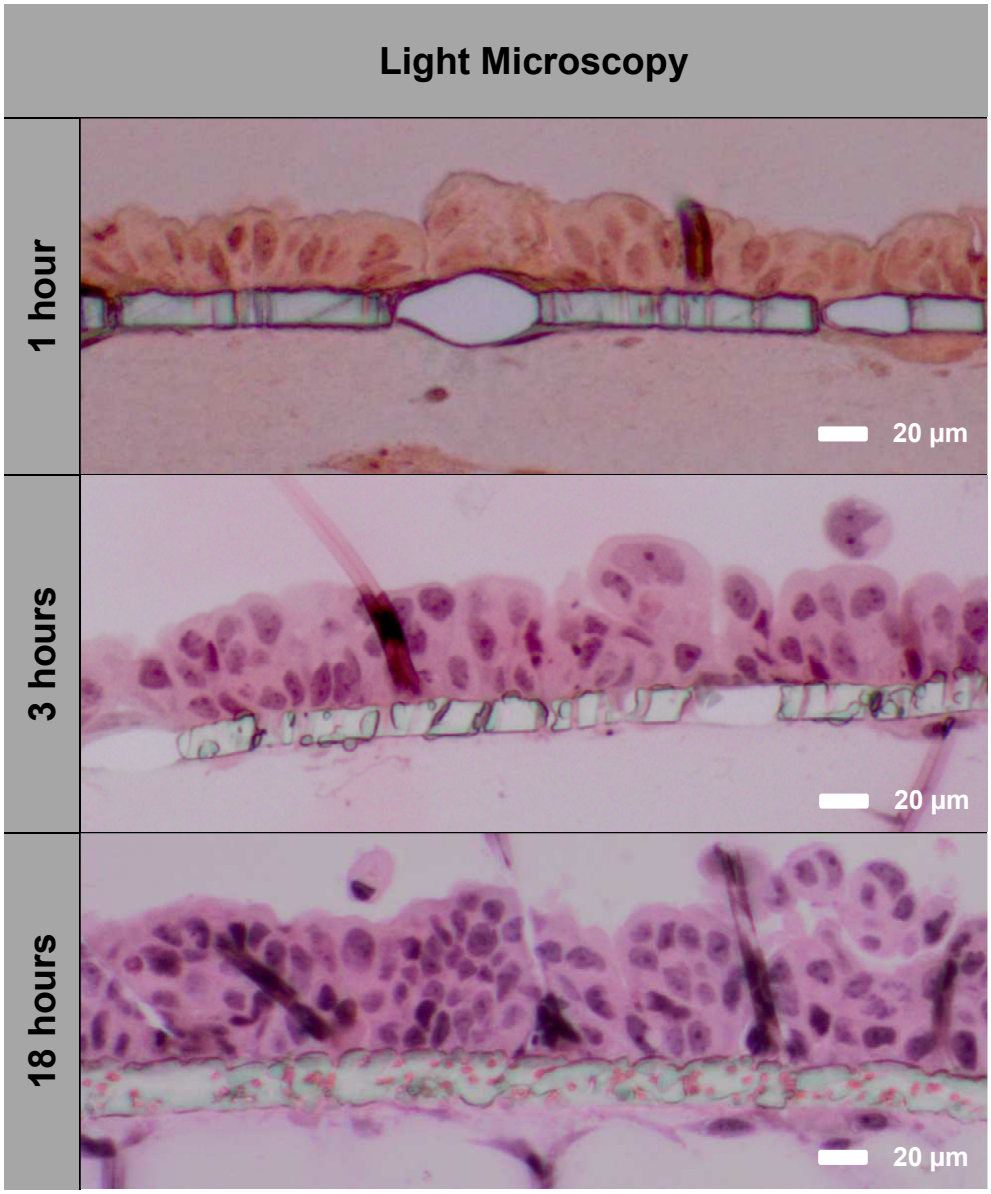

https://doi.org/10.24355/dbbs.084-201904011253-0

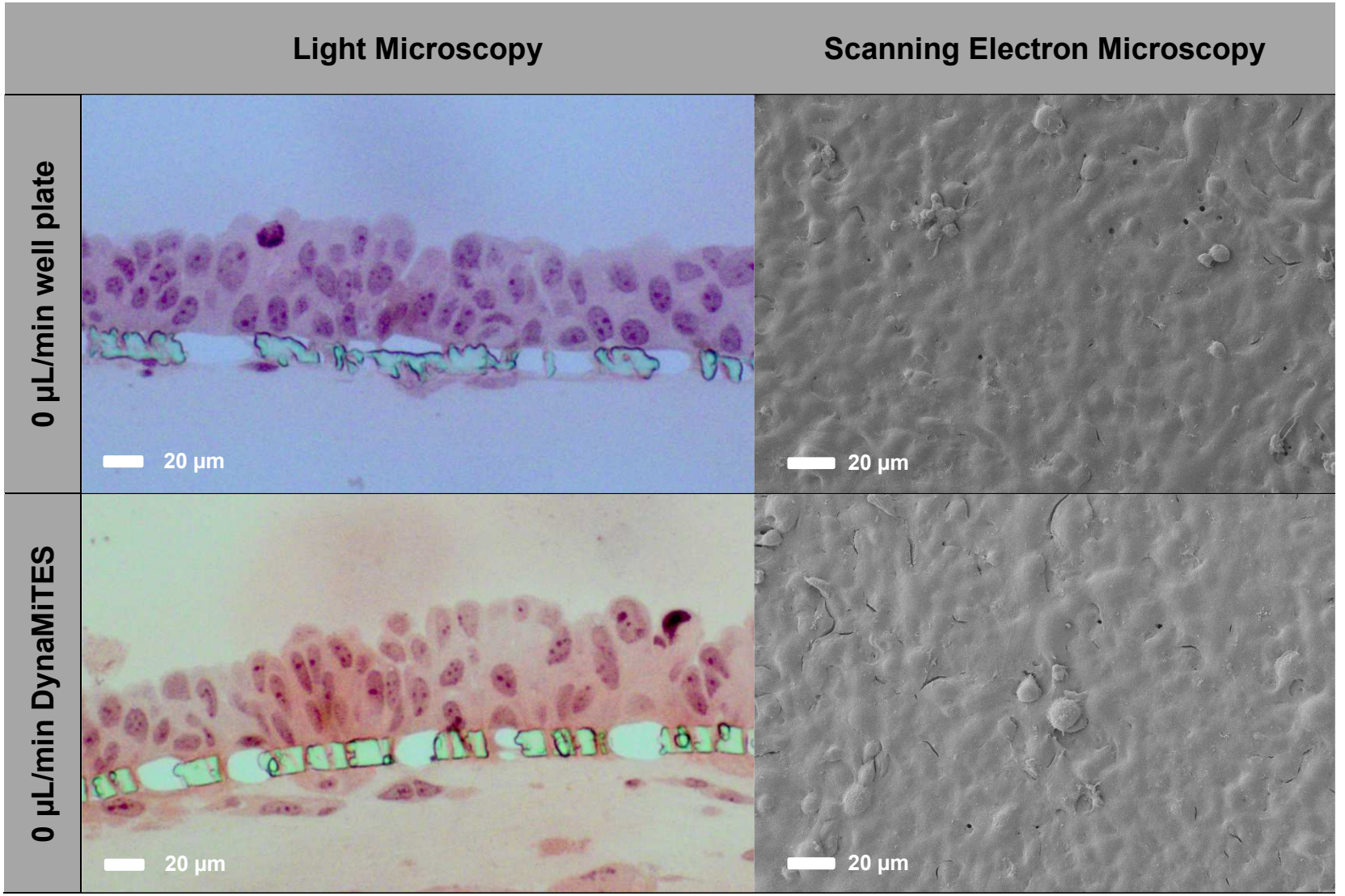

https://doi.org/10.24355/dbbs.084-201904011253-0

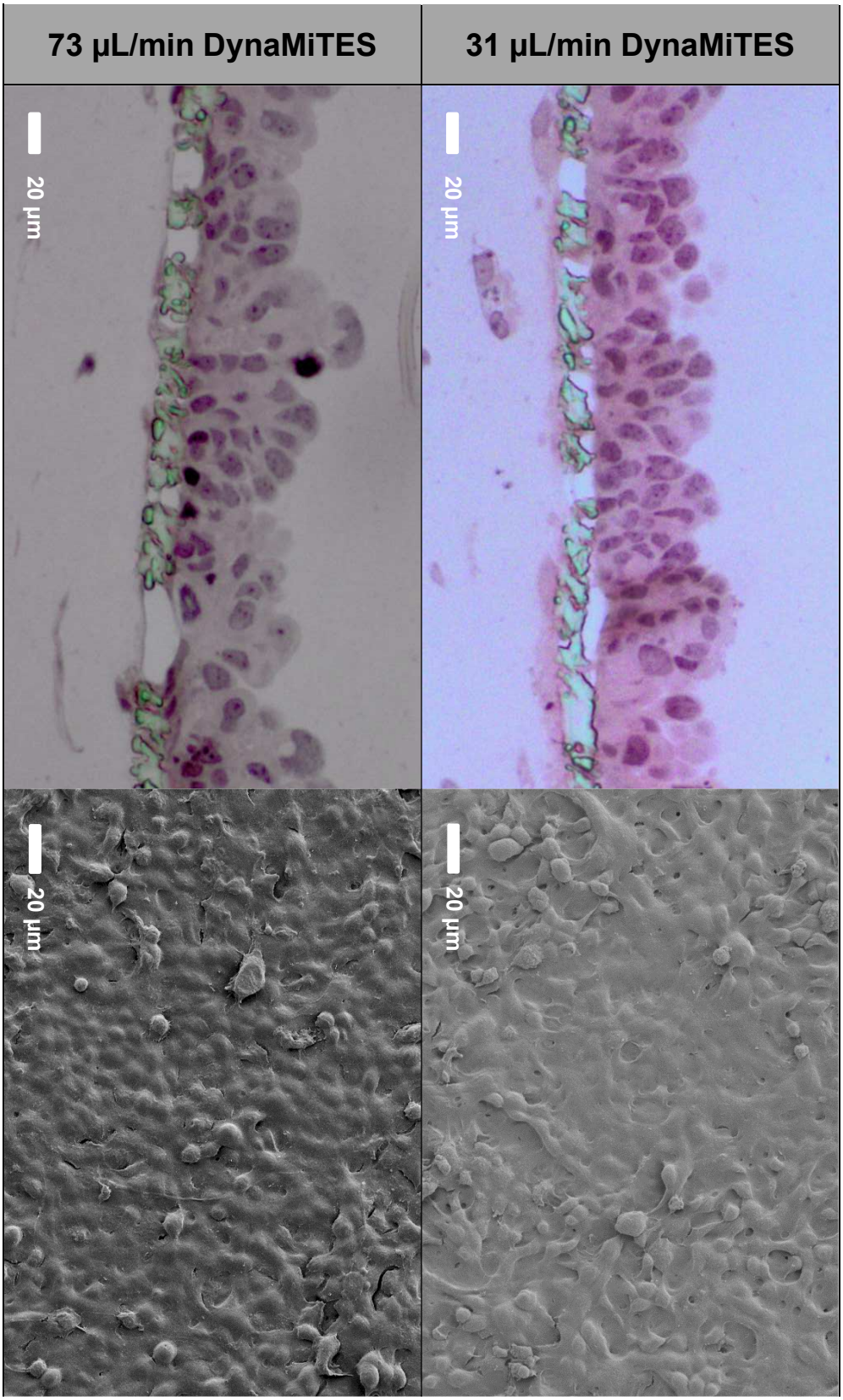

https://doi.org/10.24355/dbbs.084-201904011253-0

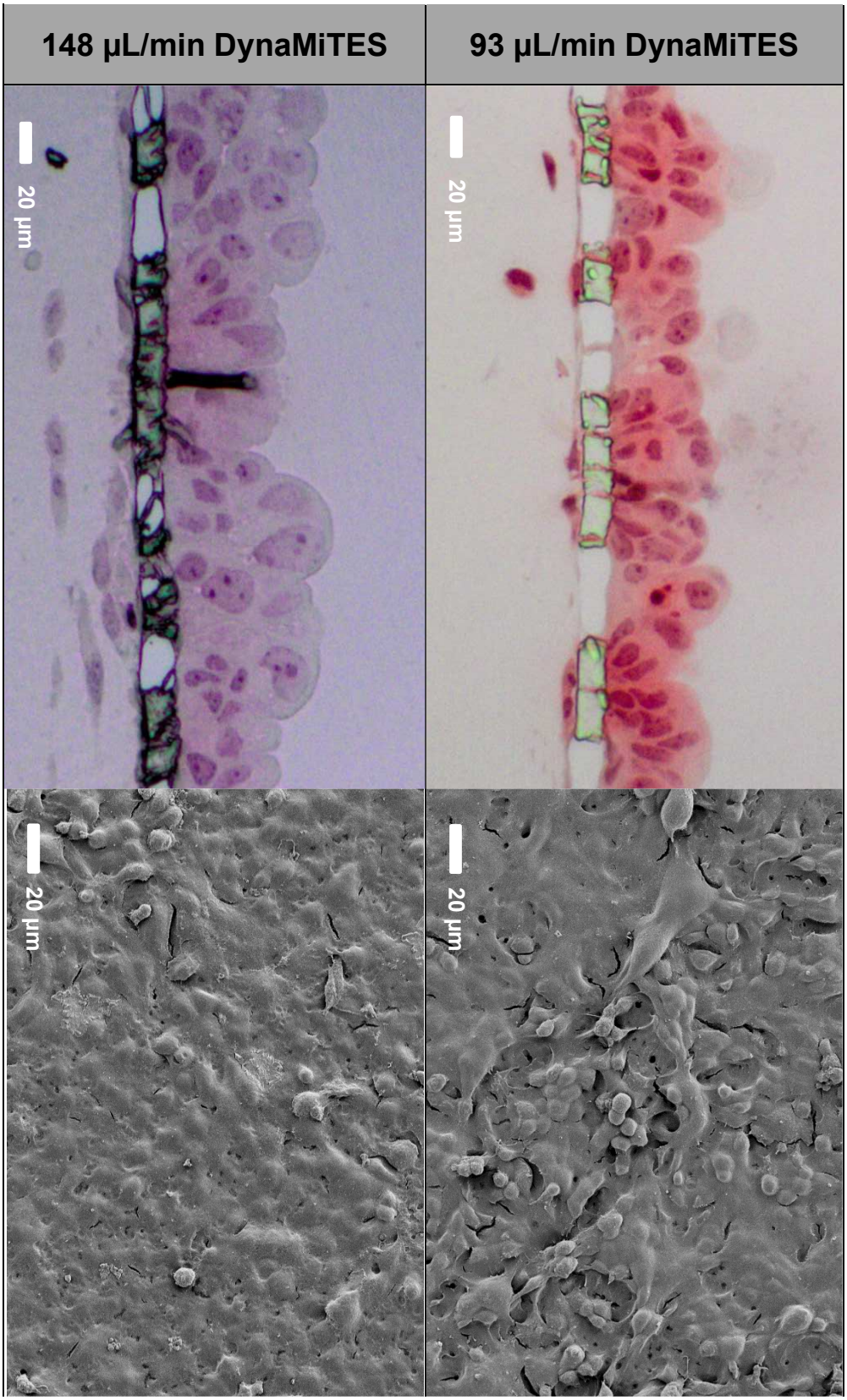

https://doi.org/10.24355/dbbs.084-201904011253-0

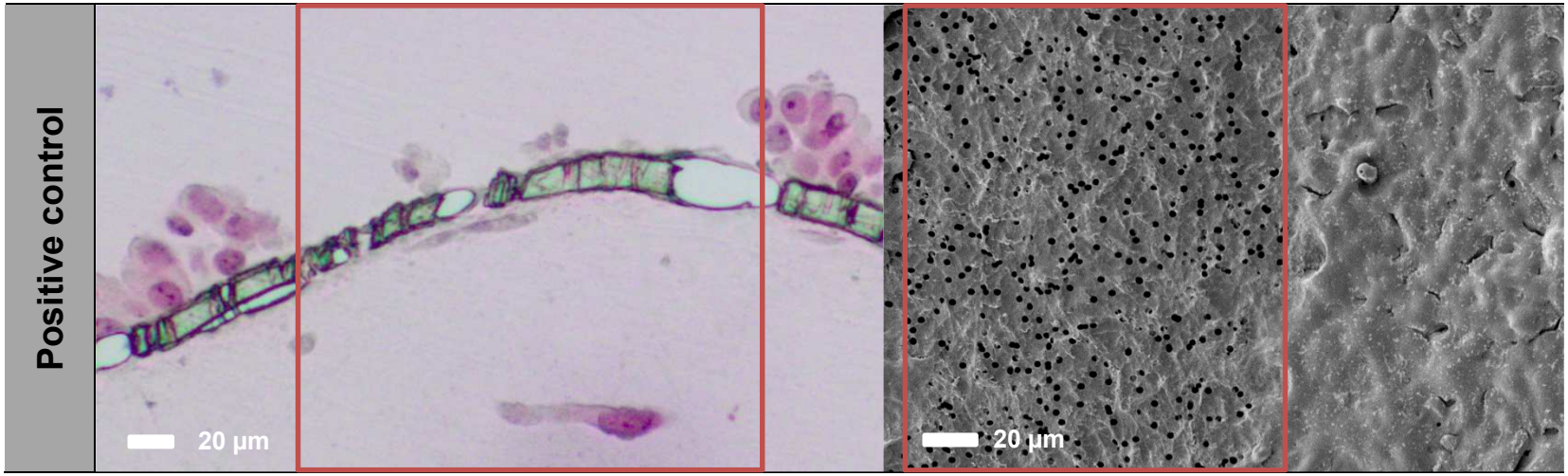

https://doi.org/10.24355/dbbs.084-201904011253-0